balt3/z1c-clinonc/z1c-clinonc/z1c99909/z1c3405-09z | xppws | S=1 | 12/23/09 | 15:33 | Art: COC200644

ORIGINAL ARTICLE

Comparison Between Conventional Surgery Plus Postoperative Adjuvant Radiotherapy and Concurrent Chemoradiation for FIGO Stage IIB Cervical Carcinoma

A Retrospective Study

AQ:1

Hideomi Yamashita, MD, Kae Okuma, ●●●,* Kei Kawana, ●●●,† Shunsuke Nakagawa, ●●●,† Katsutoshi Oda, ●●●,† Tetsu Yano, ●●●,† Shino Kobayashi, ●●●,* Reiko Wakui, ●●●,* Kuni Ohtomo, ●●●,* and Keiichi Nakagawa, ●●●**

AQ:2

Objective: To compare treatment outcome of conventional surgery followed by adjuvant postoperative radiotherapy (PORT) versus concurrent chemoradiation therapy (cCRT) for stage IIB cervical carcinoma.

Methods: A retrospective analysis was conducted of 59 patients with stage IIB uterine cervical cancer treated with radical surgery plus PORT (N = 34) or cCRT-alone (N = 25) from April 1996 to June 2008. The median follow-up time was 27 months (range, 3–150 months) in the cCRT group and 44 months (range, 4–134 months) in the PORT group. The median age was 59 years (range, 37–85 years) in the cCRT group and 49 years (range, 32–74 years) in the PORT group. All 34 patients in the surgery group underwent hysterectomy with pelvic lymph node dissection and received PORT. Twenty-five patients (42%) were assigned to the cCRT group.

Results: The 3-year overall survival rates for surgery plus PORT and cCRT-alone were 80.0% and 75.1%, respectively. The difference between these 2 treatments was not statistically significant (log-rank $P = 0.5871$). The late complication rate of grade 3–4 was 12% in the cCRT group and 16% in the surgery group.

Conclusion: This retrospective study suggests that survival results with cCRT and with conventional surgery plus PORT for patients with stage IIB cervical carcinoma are comparable.

Key Words: cervical carcinoma, surgery, chemoradiotherapy, high-dose-rate brachytherapy, stage IIB

(*Am J Clin Oncol* 2010;XX: 000–000)

Cervical cancer is the most common gynecologic malignancy in Japan, with an estimated 5 new cases per 100,000 females every year. High dose-rate intracavitary brachytherapy (HDR-ICBT) in combination with external beam irradiation (EBRT) has become an acceptable treatment for carcinoma of the cervix.[1] HDR-ICBT has been widely used in treatment of uterine cervical cancer in Asia and Europe. Although some controversy exists in the United States over the use of HDR-ICBT,[2] an increasing frequency of its adoption has been noted.[3,4]

Recently published randomized clinical trials demonstrated a significant improvement in pelvic disease control and survival when concurrent chemotherapy consisting of cisplatin-containing regimens was added to radiotherapy (RT) in patients with locally advanced cervical cancer.[5–7] These results led to significant changes in the standard treatment of cervical cancer.

Radiotherapy has long been recognized as a successful treatment modality for all stages of carcinoma of the uterine cervix. In Japan, however, because patients present first at gynecologic clinics, gynecologists usually determine the treatment modality without additional inputs from radiotherapists. In general, Japanese gynecologists consider surgical treatment to be superior to RT, and, as a result, the majority of patients with stage IIB are subjected to radical hysterectomy plus pelvic, and with or without para-aortic lymphadenectomy followed by preventive postoperative RT (PORT). Consequently, other than this preventive postoperative RT, radiation oncologists in Japan have treated only stage IIB patients who refused surgery or who were not indicated for surgery because of other coexisting disease.

Although RT has been widely used in Western countries, there are only a few reports on definitive RT for early stages (stages I–II) of cervical carcinoma. Some studies indicated that RT for early stage patients was a feasible definitive treatment.[8–11] In Japan, no prior report has compared surgery and RT. We now report the results of a retrospective study in which the survival outcomes of surgery and RT were compared for stage IIB cervical cancer. The hypothesis was to be certified that definitive cCRT is not inferior to survival and less frequency about severe complications than radical hysterectomy plus PORT for stage IIB cervical cancer in this single institution.

PATIENTS AND METHODS

Patients

Between April 1996 and June 2008, a total of 59 consecutive patients were treated for FIGO (International Federation of Gynaecology and Obstetrics classification) stage IIB carcinoma of the cervix with conventional surgery plus adjuvant PORT or concurrent CRT at our institution. All patients with stage IIB treated during the 13-year period (1996–2008) were included in the study. Patients included were those previously untreated and who had a histologic diagnosis of squamous cell carcinoma, or adenocarcinoma in FIGO stage IIB. Patients with adenocarcinoma (n = 13) were also included in this study. Median age was 53 years (range, 32–85 years). Table 1 shows the patients' characteristics. Surgically treated patients comprised 58% (34/59) and cCRT-alone patients 42% (25/59) (Table 1). The patients submitting to definitive CRT were those with comorbidities or who refused surgery in our institution. T1

Patients were evaluated with a physical and pelvic examination without anesthesia, routine blood counts, blood chemistry profile, chest radiograph, intravenous urogram, and barium enema. Computed tomography (CT) scan and magnetic resonance imaging (MRI) were used only for detecting lymphadenopathy. Pelvic and para-aortic lymph nodes greater than 10 mm in minimum diameter

From the *Departments of Radiology, and †Obstetrics and Gynecology, University of Tokyo Hospital, Tokyo, Japan.

Reprints: Hideomi Yamashita, MD, Department of Radiology, University of Tokyo Hospital, 7–3-1, Hongo, Bunkyo-ku, Tokyo 113-8655 Japan. E-mail: yamashitah-rad@h.u-tokyo.ac.jp.

ISSN: 0277-3732/10/0000-0001

DOI: 10.1097/COC.0b013e3181cae5b7

TABLE 1. Comparison of Patients' Characteristics

	Surgery Plus PORT	cCRT	*P*
Total no. patients	34	25	
Age			
Median (range) (yr)	49 (32–74)	59 (37–85)	0.0001
Histopathology			
Squamous cell carcinoma	24 (71%)	22 (88%)	0.2026
Adenocarcinoma	10 (29%)	3 (12%)	
Pelvic nodal status			
Positive	17 (50%)	5 (20%)	0.0185
Negative	17 (50%)	20 (80%)	
Paraaortic nodal status			
Positive	3 (8%)	2 (8%)	0.9106
Negative	31 (92%)	23 (92%)	
Maximum tumor diameter (mm)			
>40	19 (56%)	14 (56%)	0.9928
≦40	15 (44%)	11 (44%)	
Median (range)	49.5 (18–100)	45.5 (30–80)	0.6153

detected by CT and MRI were considered to be positive for metastases. Neither lymphangiography nor surgical evaluation of lymph nodes was performed.

Concurrent CRT

EBRT

All patients received EBRT using a linear accelerator with a photon-beam-energy of 10 MV to the whole pelvis with the 4-field box technique for a total dose of 30.6 Gy in 17 fractions (3.4 weeks, 1.8 Gy fractions from Monday to Friday). The irradiated volume was to include the whole uterus, the paracervical, parametrium and uterosacral regions, as well as the external iliac, hypogastric and obturator lymph node. Minimum margins were the upper margin of L-5 (superiorly), the lower margin of the obturator foramen or the lowest extension of the disease (inferiorly), and 2.0 cm beyond the lateral margins of the bony pelvis and its widest plane (laterally). For the lateral fields, the anterior margin was the anterior edge of the symphysis or 3 cm in front of the sacral promontory. The posterior margin was the S2–S3 interspace or the posterior border of the uterine cervix assessed by CT for treatment planning plus a 2 cm margin. After that, a midline block, 4 cm in width at midplane, was inserted with the anteroposterior parallel 2-field technique for a dose of 19.8 Gy in the last 11 fractions (ie, parametrial boost). This block extended to the top of the uterine.

Two patients who had para-aortal lymph node involvement received whole pelvic irradiation plus para-aortal irradiation using the 4-field box or conformal technique. Total dose to para-aortal lymph nodes was 50.4 Gy in 28 fractions.

ICBT

In our department, EBRT preceded ICBT. A midline block was inserted at the same time as the first application of ICBT. Four intracavitary iridium-192 (^{192}Ir) insertions were performed weekly, starting 3.4 weeks after starting EBRT. High-dose-rate intracavitary therapy was used. Brachytherapy was delivered using after-loading applicators placed in the uterine cavity and vagina. A Manchester system applicator (Nucleotron microSelectron HDR source) was used. The dose distribution was calculated for each individual patient and placement. Patients were treated in the dorsal lithotomy position. Point A was defined on radiographs as being 2 cm superior (along the tandem) to the flange abutting the external cervical os and 2 cm lateral from the axis of the tandem. Source loading corresponded to the Manchester System for uterine cervical cancer.[12] HDR-ICBT was performed once a week with a daily dose of 6 Gy at point A. The details of the method for ICBT were shown in our previous report.[13,14]

Total dose to the central area was 54.6 Gy and to the parametrium area was 50.4 Gy. When using biologically effective dose with α/β = 10 Gy, total dose to the central area was 74.5 Gy and to the parametrium was 59.5 Gy.

Chemotherapy

Concurrent CDDP-based chemotherapy combined with RT for stage IIB has been routinely performed in our department. All patients received platinum series-based chemotherapy combined with RT. All patients received CDDP (75 mg/m^2 in a bolus infusion on days 1, 22, and 43).

Surgery Plus Adjuvant RT

Radical hysterectomy with pelvic lymphadenectomy was performed on 34 patients. Radical hysterectomy at our institution includes resection of the uterus along with its attached parametrial soft tissue and a margin of the upper vagina, as in the world standard. Even when positive nodes were found, radical hysterectomy was continued without stopping. No radical hysterectomy was aborted. Para-aortic lymphadenectomy up to the level of the inferior mesenteric artery was performed for patients with adenocarcinoma or enlarged pelvic lymph nodes assessed by preoperative CT or MRI (N = 13). Because it is well-known that cases with positive pelvic lymph nodes are indicative of a very poor prognosis, lymphadenectomy up to the level of the inferior mesenteric artery was added for these high-risk cases in our institution. The median operation time was 390 minutes (range, 150–550 minutes) and the median quantity of operative blood loss was 1450 mL (range, 400–5600 mL).

All patients in the surgery group received postoperative adjuvant RT because of invasion to the parametrium. Adjuvant RT consisted of external pelvic irradiation (10 MV x-rays) with the 4-portal technique, one fraction of 1.8 Gy daily, with a total dose of 50.4 Gy over 5.6 weeks. The para-aortic region was irradiated with a dose of 50.4 Gy over 5.6 weeks with the conformal technique when metastases were detected in the surgical specimens of para-aortic nodes.

Follow-Up

Both radiation and gynecologic oncologists were involved in the follow-up the treated patients. The patients were seen every month for the first year, every 2 to 3 months for the next 2 years, and at least every 6 months thereafter. No patients were lost to follow-up. Follow-up procedures included pelvic examination, palpation of supraclavicular nodes, cervical Papanicolaou smear, and review of serum squamous cell carcinoma related antigen and cytokeratin 19 fragment antigen values. When central and/or parametrial recurrence was suspected by pelvic examination and/or Papanicolaou smear, a biopsy was taken for confirmation. Intravenously enhanced chest, abdominal, and pelvic CTs were performed annually. Other imaging studies, such as MRI, ultrasound and bone scintigraphy, were not routinely performed. Both acute and late complications were graded in accordance with the National Cancer Institute Common Toxicity Criteria Version 2.0.

Statistical Analysis

Statistical analyses were performed using StatView Dataset File version 5.0 J for Windows computers (Cary, NC). OS, progression-free survival (PFS), and local (ie, within pelvic) recurrence-free survival (LRFS) were calculated from the first date of curative treatment. Survival time was plotted using the Kaplan–Meier

method. Differences in patients' characteristics were analyzed by the χ^2 test or Fisher exact test for 2 × 2 columns and unpaired t test for a succession of numbers. Differences in survival by treatment were evaluated using the log-rank test.

RESULTS

Patients and Tumor

The age and pelvic nodal status distributions were significantly different between the 2 groups of patients (Student t test or χ^2 test). The median age was 59 years (range, 37–85 years) in the cCRT group and 49 years (range, 32–74 years) in the PORT group (Table 1). The patient FIGO stage, follow-up time, para-aortic nodal status, and histopathology distributions showed no significant differences (Table 1). The Karnofsky Performance Status for all patients was more than 80%. The proportion of patients with tumors less than 4 cm in diameter was 41% (14/34) for the surgery group and 44% (11/25) for the CRT. The median size was 50 mm (range, 18–100 mm) for the surgery group and 45.5 mm (range, 30–80 mm) for the cCRT group. The positive rate of surgical margins for the surgery group was 21% (7 cases). In the surgery group, bilateral parametrial involvement was seen in only one patient, although it was unilateral in the other 33 patients. Of those with unilateral involvement, only one patient had more than half extension of parametrial involvement and the other 32 patients had less than half.

In the surgery group, the positive rate of pelvic nodal metastasis was 32% (11 cases) assessed by clinical method and 50% (17 cases) by histopathological method. The pelvic nodal status showed no significant difference between surgery and definitive CRT groups if assessed by same method (clinically) (χ^2 test, $P = 0.2916$).

Median follow-up time was 27 months (range, 3–150 months) in the cCRT group and 44 months (range, 4–134 months) in the PORT group. The proportion of the surviving patients was 74% (25/34) for the surgery and 76% (19/25) for the cCRT groups.

The first site of progression was local-alone (ie, within pelvis) in 8% (2 cases) for the definitive CRT group and in 12% (4 cases) for the surgery group. Additionally, it was distant-alone progression in 4% (1 case) for CRT group and in 18% (6 cases) for surgery group, and both local and distant in 8% (2 cases) for CRT group and 0% for the surgery group. In other words, the recurrent rate within the pelvis was 14% (8/59 cases).

Survival

When this analysis was closed, 44 of 59 patients were alive. Deaths resulted in all 15 patients with cervical cancer (6 patients for definitive CRT group and 9 patients for surgery group). No treatment-related deaths were encountered. Figure 1 shows a comparison of the OS curves for the definitive CRT and surgery groups. The 3-year OS rates were 75% for the cCRT group and 80% for the surgery, respectively; the difference between these 2 rates was not significant (log-rank $P = 0.5871$). The 3-year PFS rates were 79% for the cCRT group and 70% for the surgery, respectively ($P = 0.7247$, HR = 0.825, 95% CI = 0.281–2.422). The 3-year LRFS rate was 83% for the cCRT group and 86% for the surgery, respectively ($P = 0.4908$, HR = 1.622, 95% CI = 0.404–6.513). Clearly, none of these analyses was of any significance.

Complications

In the cCRT group, nonhematological acute toxicity and all late toxicity (complications that persisted or occurred for more than 60 days after treatment) of grade 3+ were noted in 3 patients (12%). Small bowel perforation without tumor recurrence (grade 4) and melena from radiation proctitis in 2 cases (both grade 3) were seen at 5, 8, and 11 months after the completion of CRT. Moreover, grades 1 or 2 melena and lymphoedema of the lower limbs were seen in each of 4 patients (16%).

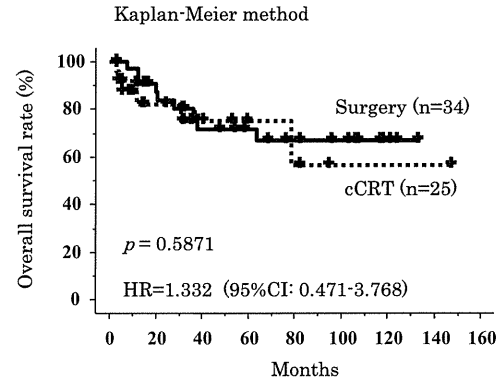

FIGURE 1. Overall survival curves in stage IIB patients comparing surgery plus postoperative radiotherapy (surgery) and concurrent chemoradiation (cCRT).

In the surgery group, the bladder damage was seen in one example for a complication during operation. Nonhematological acute toxicity of grade 3+ was seen in 9 patients (16%). Postoperative ileus (grade 4 in 1 patient and grade 3 in 3 patients), grade 3 pelvic lymphocyst in one patient, grade 3 pulmonary infarction in 2 patients, grade 3 bilateral hydronephrosis in one patient, and lymphangitis of lower extremities (grade 3) in one patient were seen. Moreover, grade 2 hypertension, urinary tract infection, unilateral functionless kidney, and pelvic lymphocyst were seen in each of a single patient (total was 16%). No ureteral stricture was seen in the neither PORT or surgery groups.

DISCUSSION

This is a retrospective analysis of 59 patients with FIGO stage IIB cervical cancer treated with surgery plus PORT (n = 34) or concomitant CRT-alone (n = 25). Some centers especially in Japan still consider both treatment modalities as a standard for FIGO stage IIB cervical cancer. In this study, the 3-year OS, PFS, and LRFS were the same for both groups, although the surgery cases had at least a debulking of lymph nodes when positive as compared with the definitive CRT group. Also, CRT patients received a slight low dose for tumor control: only 50.4 Gy with EBRT plus 4 × 6 Gy with HDR-ICRT. These techniques are quite different from those used to treat the same category of patients in the United States and Europe. Additionally, surgery plus PORT presented 16% of grade 3+ complications. Patients who received definitive CRT were at higher risk, when age and probable comorbidities were considered. This suggests that there is no treatment of choice with respect to local control of disease. Conceivably, the patient population might be too small to draw any conclusions about the superiority of either one of the 2 treatment modalities.

The type of radical hysterectomy performed was III and ureteral resection was performed, although we had 21% of positive margins. The median and mean number of excised nodes was 61 and 63.4 (range, 25–133).

Many previously published results[8–11,15,16] suggest that radical hysterectomy or definitive RT is standard treatments for IB–IIA. In the United States and Europe, definitive RT has been selected in many cases. Radical hysterectomy is not a world standard for stage IIB patients. In contrast, surgery is preferentially used over RT in Japan even for stage IIB cervical cancer, although those patients with stage IIB ideally should have been treated with concomitant

CRT. RT is usually selected only for the elderly or inoperable cases because of coexisting disease in Japan.

The age of the patients and pelvic nodal status were significantly different between those patients going to surgery and cCRT patients (Table 1). The mean age of the cCRT patients was significantly greater than that of patients in the surgery group ($P = 0.0001$). There was a tendency for cCRT to be performed for elderly patients who were fearful of surgery or general anesthesia. Regardless of these fears, the cCRT patients had survival rates comparable with the surgery patients.

For the surgery group, pelvic nodal status was pathologically assessed in the surgical specimen, whereas clinically assessed by CT or MRI in the cCRT group. The positive rate of pelvic nodal status for the surgery group was significantly higher than in the cCRT group (50% vs. 20%, $P = 0.0185$). In the surgery group, the positive rate of pelvic nodal metastasis was 32% (11 cases) assessed clinically. The pelvic nodal status showed no significant difference between surgery and definitive CRT groups if assessed by the same method (clinically) (χ^2 test, $P = 0.2916$).

Horn et al[17] concluded that tumor size, when bulky disease was defined as tumors larger than 4 cm, was also of prognostic importance in FIGO stage II cervical carcinomas. In this study, there was no significant difference in the maximum tumor diameter between the 2 groups ($P = 0.6153$), although stage IIB varied from minimal to medial and even to lateral parametrial invasions, just short of pelvic wall fixation. To determine the size of the tumor, pathologic evaluation was used in the PORT group and pretreatment MRI in the CRT group.

Rotman et al[18] concluded that pelvic RT after radical surgery significantly reduced the risk of recurrence and prolonged PFS in women with stage IB cervical cancer whereas PORT appeared to be particularly beneficial for patients with tumors comprised of adenocarcinoma or adenosquamous histologies. In this study, there was no significant difference in the number of adenocarcinomas between the 2 groups ($P = 0.2026$).

It was shown in a previous publication[19] that for the stage IIB patients with lateral parametrial involvement had significantly higher rates of pelvic failure and of survival in comparison with those patients with medial parametrial involvement.

In our experience, the low rate of major complications after cCRT suggests that this approach is well tolerated in most patients. Treatment-related toxicity of grade 3+ developed in 16% of the surgery patients and in 12% of the definitive CRT group. This difference was not significant, probably because of the small numbers of patients in both groups.

Our results confirm earlier findings that have suggested that cCRT is not inferior to surgery plus PORT for FIGO stage IIB cervical carcinoma regardless of age bias, although the 2 treatment groups were not similar (ie, the cCRT group was older and had more comorbidities) and the pelvic node status was different as well. The 3-year outcomes in both groups were also been shown to be compatible with previous reports.[2–8] Because the t test based on a sample of 59 is underpowered, clinical trails with more patients should be needed to further confirm the efficacy of cCRT or surgery plus PORT on FIGO stage IIB cervical carcinoma. By the power analysis, to detect the difference between 2 independent groups, when the input is assumed that tail = one, effect size r = 0.5 (large), 0.3 (medium), or 0.1 (small), α err probability = 0.05, power (1-β err probability) = 0.8, and allocation ratio N2/N1 = 1, total sample size is calculated as 102, 278, or 2476, respectively. This study is too underpowered to conclude whether such both techniques as radical hysterectomy plus PORT and definitive CRT are feasible.

In this study, it was to be certified that definitive cCRT is not inferior with regards to survival and less frequency about severe complications than radical hysterectomy plus PORT for stage IIB cervical cancer in this single institution. The limitations of our study included the retrospective nature of the study, heterogeneity of the patient population in the 2 treatment arms, shorter follow-up and physician's bias in the selection of the patients. A matched-pair analysis would be better to compare the 2 groups but could not be done in our study because of the small number of patients. Nevertheless, we hope that our experience will initiate further prospective studies especially in Japan.

REFERENCES

1. Morita K. Cancer of the cervix. In: Vahrson HW, ed. *Radiation Oncology of Gynecological Cancers*. Berlin, Germany: Springer; 1997:143–239.
2. Eifel PJ. High-dose-rate brachytherapy for carcinoma of the cervix: high tech or high risk? *Int J Radiat Oncol Biol Phys*. 1992;24:383–386.
3. Eifel PJ, Moughan J, Owen J, et al. Patterns of radiotherapy practice for patients with squamous carcinoma of the uterine cervix: patterns of care study. *Int J Radiat Oncol Biol Phys*. 1999;43:351–348.
4. Nag S, Orton C, Young D, et al. The American brachytherapy society survey of brachytherapy practice for carcinoma of the cervix in the United States. *Gynecol Oncol*. 1999;73:111–118.
5. Rose PG, Bundy BN, Watkins EB, et al. Concurrent cisplatin-based chemotherapy and radiotherapy for locally advanced cervical cancer. *N Engl J Med*. 1999;340:1144–1153.
6. Whitney CW, Sause W, Bundy BN, et al. A randomized comparison of fluorouracil plus cisplatin versus hydroxyurea as an adjunct to radiation therapy in stages IIB–IVA carcinoma of the cervix with negative para-aortic lymph nodes: a Gynecologic Oncology Group and Southwest Oncology Group study. *J Clin Oncol*. 1999;17:1339–1348.
7. Morris M, Eifel PJ, Lu J, et al. Pelvic radiation with concurrent chemotherapy compared with pelvic and paraaortic radiation for high-risk cervical cancer. *N Engl J Med*. 1999;340:1137–1143.
8. Eifel PJ, Morris M, Wharton JT, et al. The influence of tumor size and morphology on the outcome of patients with FIGO stage IB squamous cell carcinoma of the uterine cervix. *Int J Radiat Oncol Biol Phys*. 1994;29:9–16.
9. Horiot JC, Pigneux J, Pourquier H, et al. Radiotherapy alone in carcinoma of the intact uterine cervix according to G. H. Fletcher guidelines: a French cooperative study of 1383 cases. *Int J Radiat Oncol Biol Phys*. 1988;14:605–611.
10. Liu W, Meigs JV. Radical hysterectomy and pelvic lymphadenectomy. A review of 473 cases including 244 for primary invasive carcinoma of the cervix. *Am J Obstet Gynecol*. 1955;69:1–32.
11. Newton M. Radical hysterectomy or radiotherapy for stage I cervical cancer. *Am J Obstet Gynecol*. 1975;123:535–542.
12. Tod MC, Meredith WJ. A dosage system for use in the treatment of cancer of the uterine cervix. *Br J Radiol*. 1938;11:809–824.
13. Yamashita H, Nakagawa K, Tago M, et al. Treatment results and prognostic analysis of radical radiotherapy for locally advanced cancer of the uterine cervix. *Br J Radiol*. 2005;78:821–826.
14. Yamashita H, Nakagawa K, Tago M, et al. Comparison between conventional surgery and radiotherapy for FIGO stage I–II cervical carcinoma: a retrospective Japanese study. *Gynecol Oncol*. 2005;97:834–839.
15. Morley GW, Seski JC. Radical pelvic surgery versus radiation therapy for stage I carcinoma of the cervix (exclusive of microinvasion). *Am J Obstet Gynecol*. 1976;126:785–798.
16. Landoni F, Maneo A, Colombo A, et al. Randomized study of radical surgery versus radiotherapy for stage Ib–IIa cervical cancer. *Lancet*. 1997;350:535–540.
17. Horn LC, Fischer U, Raptis G, et al. Tumor size is of prognostic value in surgically treated FIGO stage II cervical cancer. *Gynecol Oncol*. 2007;107:310–315.
18. Rotman M, Sedlis A, Piedmonte MR, et al. A phase III randomized trial of postoperative pelvic irradiation in Stage IB cervical carcinoma with poor prognostic features: follow-up of a gynecologic oncology group study. *Int J Radiat Oncol Biol Phys*. 2006;65:169–176.
19. Perez CA, Grigsby PW, Chao KS, et al. Tumor size, irradiation dose, and long-term outcome of carcinoma of uterine cervix. *Int J Radiat Oncol Biol Phys*. 1998;41:307–317.

Infection and Immunity

Nanogel-Based PspA Intranasal Vaccine Prevents Invasive Disease and Nasal Colonization by Streptococcus pneumoniae

Il Gyu Kong, Ayuko Sato, Yoshikazu Yuki, Tomonori Nochi, Haruko Takahashi, Shinichi Sawada, Mio Mejima, Shiho Kurokawa, Kazunari Okada, Shintaro Sato, David E. Briles, Jun Kunisawa, Yusuke Inoue, Masafumi Yamamoto, Kazunari Akiyoshi and Hiroshi Kiyono

Infect. Immun. 2013, 81(5):1625. DOI: 10.1128/IAI.00240-13.
Published Ahead of Print 4 March 2013.

IAI
Journals.ASM.org

Nanogel-Based PspA Intranasal Vaccine Prevents Invasive Disease and Nasal Colonization by *Streptococcus pneumoniae*

Il Gyu Kong,[a,b,c] Ayuko Sato,[a,d] Yoshikazu Yuki,[a,d] Tomonori Nochi,[e] Haruko Takahashi,[f] Shinichi Sawada,[f] Mio Mejima,[a] Shiho Kurokawa,[a] Kazunari Okada,[a,d] Shintaro Sato,[a,d] David E. Briles,[g] Jun Kunisawa,[a,d,h,i] Yusuke Inoue,[j] Masafumi Yamamoto,[k] Kazunari Akiyoshi,[f] Hiroshi Kiyono[a,b,d,h]

Division of Mucosal Immunology, Department of Microbiology and Immunology,[a] and International Research and Development Center for Mucosal Vaccines,[h] The Institute of Medical Science, The University of Tokyo, Tokyo, Japan; Graduate School Medicine and Faculty of Medicine, The University of Tokyo, Tokyo, Japan[b]; Department of Otorhinolaryngology, Seoul National University College of Medicine, Seoul, South Korea[c]; Core Research for Evolutional Science and Technology (CREST), Japan Science and Technology Agency, Tokyo, Japan[d]; Division of Infectious Diseases, Center for AIDS Research, University of North Carolina School of Medicine, Chapel Hill, North Carolina, USA[e]; Department of Polymer Chemistry, Kyoto University Graduate School of Engineering, Kyoto, Japan[f]; Department of Microbiology, University of Alabama at Birmingham, Birmingham, Alabama, USA[g]; Laboratory of Vaccine Materials, National Institute of Biomedical Innovation, Osaka, Japan[i]; Department of Diagnostic Radiology, Kitasato University School of Medicine, Kanagawa, Japan[j]; Department of Microbiology and Immunology, Nihon University School of Dentistry at Matsudo, Chiba, Japan[k]

To establish a safer and more effective vaccine against pneumococcal respiratory infections, current knowledge regarding the antigens common among pneumococcal strains and improvements to the system for delivering these antigens across the mucosal barrier must be integrated. We developed a pneumococcal vaccine that combines the advantages of pneumococcal surface protein A (PspA) with a nontoxic intranasal vaccine delivery system based on a nanometer-sized hydrogel (nanogel) consisting of a cationic cholesteryl group-bearing pullulan (cCHP). The efficacy of the nanogel-based PspA nasal vaccine (cCHP-PspA) was tested in murine pneumococcal airway infection models. Intranasal vaccination with cCHP-PspA provided protective immunity against lethal challenge with *Streptococcus pneumoniae* Xen10, reduced colonization and invasion by bacteria in the upper and lower respiratory tracts, and induced systemic and nasal mucosal Th17 responses, high levels of PspA-specific serum immunoglobulin G (IgG), and nasal and bronchial IgA antibody responses. Moreover, there was no sign of PspA delivery by nanogel to either the olfactory bulbs or the central nervous system after intranasal administration. These results demonstrate the effectiveness and safety of the nanogel-based PspA nasal vaccine system as a universal mucosal vaccine against pneumococcal respiratory infection.

The use of polysaccharide-based injectable multivalent pneumococcal conjugate vaccines (PCV7, -10, and -13) has diminished the number of fatal infections due to pneumococci expressing the particular polysaccharides present in the vaccine (1–3). However, *Streptococcus pneumoniae* remains a problematic pathogen (4, 5) because of the large number of different capsular polysaccharides associated with virulent disease in humans. In particular, nonvaccine strains are emerging pathogens that result in morbidity and mortality due to pneumococcal diseases, including pneumonia and meningitis (6–8).

Clinical demand to overcome these problems has prompted the preclinical development of universal serotype-independent pneumococcal vaccines that are based on a surface protein common to all strains. Pneumococcal surface protein A (PspA), a pneumococcal virulence factor (9–13), is genetically variable (14) but highly cross-reactive (9, 10). PspA is commonly expressed by all capsular serotypes of *S. pneumoniae* (15) and is classified into 3 families (family 1, clades 1 and 2; family 2, clades 3 through 5; and family 3, clade 6) according to sequence similarities (14). Given that parenteral immunization with PspA induces cross-reactive neutralizing immune responses in mice (16–18) and humans (19), using PspA as a serotype-independent common antigen for the development of pneumococcal vaccines seems to be an ideal strategy.

Pneumococcal infection is generally preceded by colonization of the upper airway (20, 21). Nasal carriage of pneumococci is the primary source for spread of the infection among humans (22, 23). Therefore, an optimal vaccine strategy to prevent and control the spread of pneumococcal disease would induce protective immunity against both colonization and invasive disease. Several studies have confirmed the efficacy of PspA as a nasal vaccine antigen by coadministering PspA with a mucosal adjuvant such as cholera toxin (CT) or cholera toxin subunit B (CTB) to mice (24–26). The mice subsequently mount antigen-specific immune responses in not only the systemic compartment but also the respiratory mucosal compartment (24, 25, 27), where bacterial colonization occurs (20). PspA-specific secretory immunoglobulin A (sIgA) antibodies induced by intranasal immunization with PspA and an adjuvant (i.e., a plasmid expressing Flt3 ligand cDNA) provide protection against pneumococcal colonization (28). In addition, studies in mice have revealed that this protection is mediated by antigen-specific interleukin 17A (IL-17A)-secret-

Received 20 February 2013 **Accepted** 21 February 2013
Published ahead of print 4 March 2013
Editor: R. P. Morrison
Address correspondence to Hiroshi Kiyono, kiyono@ims.u-tokyo.ac.jp, or Yoshikazu Yuki, yukiy@ims.u-tokyo.ac.jp.
Supplemental material for this article may be found at http://dx.doi.org/10.1128/IAI.00240-13.

doi:10.1128/IAI.00240-13

ing $CD4^+$ T cells induced by intranasal immunization with pneumococcal whole-cell antigen (29, 30).

Therefore, the intranasal vaccination route is an improved route for preventing colonization of the nasal cavity by pneumococci. A leading obstacle to the practical use of nasal vaccine with a protein-based pneumococcal antigen is the need to coadminister a toxin-based mucosal adjuvant (e.g., CT) for effective induction of antigen-specific immune responses (31, 32). However, the use of such toxin-based adjuvants is undesirable in humans, as it carries the concern that the toxin may reach the central nervous system (CNS) or redirect the vaccine antigen into the CNS through the olfactory nerve in the nasal cavity (33, 34). To bypass these concerns, we recently developed a nasal vaccine delivery system based on a non-toxin-based mucosal antigen carrier, a cationic cholesteryl pullulan (cCHP) nanogel (35).

Here we show the efficacy of a nanogel-based nasal pneumococcal vaccine in which PspA is incorporated into a cCHP nanogel (cCHP-PspA). We also characterized the cCHP-PspA-induced PspA-specific Th17 and antibody responses against *S. pneumoniae*. Mice immunized with nasal cCHP-PspA were protected from lethal challenge with *S. pneumoniae* and had fewer pneumococci on their respiratory mucosae. These results suggest that a nontoxic nasal vaccine comprising nanogel-based PspA offers a practical and effective strategy against pneumococcal infection by preventing both nasal colonization and invasive diseases.

MATERIALS AND METHODS

Mice. Female BALB/c mice (aged 6 to 7 weeks) were purchased from SLC (Shizuoka, Japan). All of the mice were housed with *ad libitum* food and water on a standard 12-h–12-h light-dark cycle. All experiments were performed in accordance with the guidelines provided by the Animal Care and Use committees of the University of Tokyo and were approved by the Animal Committee of the Institute of Medical Science of the University of Tokyo.

Recombinant PspA. Recombinant PspA of *S. pneumoniae* Rx1, which belongs to PspA family 1, clade 2 (14), was prepared as described previously, with slight modifications (26). Briefly, a plasmid encoding PspA/Rx1 (pUAB055; amino acids 1 through 302) (GenBank accession no. M74122) was used to transform *Escherichia coli* BL21(DE3) cells. This construct contains amino acids 1 through 302 of the PspA protein from strain Rx1 plus a 6×His tag at the C terminus (26). The sonicated cell supernatant was loaded onto a DEAE-Sepharose column (BD Healthcare, Piscataway, NJ) and a nickel affinity column (Qiagen, Valencia, CA). This was followed by gel filtration on a Sephadex G-100 column (BD Healthcare).

Preparation of cCHP-recombinant PspA complex for intranasal vaccination. A cCHP nanogel (size, ~40 nm) generated from a cationic cholesteryl group-bearing pullulan was used for all experiments. The cCHP-PspA complex for each immunization was prepared by mixing 7.5 μg PspA with cCHP at a 3:1 molecular ratio (volume, 18 μl per mouse) and incubating the mixture for 1 h at 45°C. Before the complex was used in *in vivo* studies, the fluorescence resonance energy transfer (FRET) of fluorescein isothiocyanate (FITC)-PspA and a tetramethyl rhodamine isothiocyanate (TRITC)-cCHP nanogel was measured with a fluorescence spectrometer (model FP-6500; Jasco, Easton, MD) as described previously (37). FRET analyses confirmed that the cCHP nanogel appropriately formed nanoparticles after the incorporation of PspA (see Fig. S1 in the supplemental material). Dynamic light scattering analysis showed that the cCHP nanogel maintained the same nanoscale size (32.8 ± 0.2 nm) even after the incorporation of PspA. Lipopolysaccharide (LPS) contamination of purified PspA and cCHP (<10 endotoxin units/mg protein) was measured with a *Limulus* test (Wako, Osaka, Japan).

Immunization. Once weekly for 3 consecutive weeks, female BALB/c mice were immunized intranasally with cCHP-PspA, PspA plus CT (1 μg; List Biological Laboratory, Campbell, CA), PspA alone, or phosphate-buffered saline (PBS) only. Some experiments included an irrelevant antigen as a control; in these studies, mice were immunized intranasally with a complex of cCHP nanogel and a recombinant nontoxic receptor-binding fragment of *Clostridium botulinum* type A neurotoxin subunit antigen Hc (cCHP-BoHc/A) (35). Serum, nasal wash fluid (NW), and bronchoalveolar lavage fluid (BALF) samples were harvested 1 week after the last immunization. For NWs, 200 μl sterile PBS was flushed through the posterior choanae (38). BALF was harvested by instilling 1 ml of sterile PBS through a blunt needle placed in the trachea (38).

Bacterial strain. We used the kanamycin-resistant pneumococcal strain *S. pneumoniae* Xen10 (Caliper Life Sciences, MA), derived from the wild-type strain A66.1, which expresses PspA of family 1, clades 1 and 2 (39). *S. pneumoniae* Xen10 carries a stable copy of the modified *Photorhabdus luminescens lux* operon at a single integration site on the bacterial chromosome (40). The virulence of *S. pneumoniae* Xen10 is comparable to that of the parent strain (40, 41). For challenge studies, *S. pneumoniae* 3JYP3670, which expresses PspA of family 2, clade 4, was used (10). All of the *S. pneumoniae* strains were grown in brain heart infusion (BHI) broth at 37°C in 5% CO_2.

Pneumococcal infection model. To evaluate the efficacy of intranasal vaccination with cCHP-PspA, mice were challenged 1 week after the last immunization. The cell densities of exponentially growing *S. pneumoniae* Xen10 cultured at 37°C in BHI broth were estimated from the optical density at 600 nm (OD_{600}); cells were pelleted and then diluted with PBS. Lethal (2×10^5 CFU) and sublethal (2×10^4 CFU) challenge doses diluted in 50 μl sterile PBS were administered intranasally to isoflurane-anesthetized mice. Mice were restrained vertically for 5 min to ensure inhalation of the organisms into the trachea. In addition, mice were inoculated intranasally with a lethal challenge dose (5×10^4 CFU) of strain 3JYP3670 in the same way as that for strain Xen10. Nasal passages and lung tissues were homogenized in 500 μl sterile PBS for 1 min, and the numbers of bacterial colonies were determined by plating samples on LB agar plates containing kanamycin (200 μl/ml).

***In vivo* imaging of immunized and challenged mice.** Bioluminescence of bacteria was monitored for 1 min 24, 48, and 72 h after lethal challenge by using an Ivis charge-coupled device (CCD) camera (Xenogen, Alameda, CA). Total photon emission from the entire thorax of each mouse was quantified by using the LivingImage software package (Xenogen). The results are provided as numbers of photons/s/cm^2/sr.

Antibody titer and subclass analysis. Antibody titers were determined by using enzyme-linked immunosorbent assay (ELISA) as described previously, with slight modifications (25). In brief, samples (2-fold serial dilutions) were loaded into individual wells, and the plate was coated with 1 μg/ml recombinant PspA and incubated. Goat anti-mouse IgA, IgG, IgG1, IgG2a, IgG2b, IgG3, and IgM (dilution factor, 1:4,000) conjugated with horseradish peroxidase were used as secondary antibodies. Reactions were visualized by using the TMB microwell peroxidase substrate system (XPL, Gaithersburg, MD). The endpoint titer is expressed as the reciprocal $\log_2$ of the last dilution that gave an OD_{450} that was 0.1 unit greater than that of the negative control.

PspA-specific $CD4^+$ T cell responses. By using anti-CD4 microbeads (Miltenyi Biotec, Sunnyvale, CA) according to the manufacturer's instructions, $CD4^+$ T cells were isolated from the spleens and cervical lymph nodes (CLNs) of mice intranasally immunized with cCHP-PspA, PspA alone, or PBS only. The purified $CD4^+$ T cells were resuspended at 1×10^6 cells/ml in RPMI 1640 (Cellgro, Mediatech, Washington, DC) supplemented with 10 mM HEPES, 50 μM 2-mercaptoethanol, 100 U/ml penicillin, 100 μl/ml streptomycin, and 10% fetal calf serum and then cocultured with irradiated (2,000 rad) splenic antigen-presenting cells (2×10^6 cells/ml) from naïve BALB/c mice for 5 days at 37°C in 5% CO_2 in the presence of 1 μg/ml PspA. Cytokine levels in $CD4^+$ T cell culture supernatants were determined by using cytokine-specific DuoSet ELISA kits

(R&D Systems, Minneapolis, MN) according to the manufacturer's instructions.

Radioisotope counting assay. To trace the distribution of PspA after intranasal immunization, PspA was labeled with indium chloride (Nihon Medi-Physics, Tokyo, Japan) anhydride (Dojindo, Kumamoto, Japan) via N-terminal and ε-Lys amino groups, using diethylenetriaminepentaacetic acid as described previously (42). ^{111}In-labeled PspA was administered alone or as a complex with cCHP nanogel. The radioisotope counts in the nasal passage, olfactory bulbs, and brain 10 min and 1, 6, 12, 24, and 48 h after instillation were estimated with a γ-counter (Wizard model 1480; PerkinElmer, Waltham, MA). The results are provided as standardized uptake values (SUVs), calculated as radioisotope counts (cpm) per gram of tissue divided by the ratio of the injected dose (1×10^6 cpm) to body weight (in grams).

Flow cytometric analysis. Mice were immunized intranasally with FITC-PspA in cCHP nanogel, FITC-PspA alone, or PBS only; 6 h later, mononuclear cells were prepared from the nasal passages of each group by mechanical dissociation through 70-μm nylon mesh, as described previously (38, 43). Isolated cells were stained with phycoerythrin (PE)-Cy7-conjugated anti-CD11c (BD Bioscience) and analyzed by flow cytometry. The percentage of PspA$^+$ cells in the CD11c$^+$ fractions was calculated for each experimental group.

Data analysis. Data are expressed as means ± standard deviations (SD). Statistical analysis for most comparisons among groups was performed with Tukey's *t* test; differences were considered statistically significant when the *P* value was <0.05. For survival data, the Fisher exact test was used to compare the numbers of alive versus dead mice in the cCHP-PspA, PspA-CT, and PBS-only groups with those in the PspA-only group.

RESULTS

Intranasal vaccination with cCHP-PspA induces protective immunity against lethal challenge with *S. pneumoniae*. To evaluate whether intranasal cCHP-PspA vaccination induces protective immunity against pneumococcal challenge, we vaccinated mice with cCHP-PspA, PspA-CT, PspA alone, or PBS only. One week after the last immunization, we lethally challenged vaccinated mice with the virulent strain *S. pneumoniae* Xen10 (2×10^5 CFU), which is *S. pneumoniae* A66.1 rendered bioluminescent by the integration of a modified *lux* operon into its chromosome (40). The PspA expression level of strain Xen10 was confirmed to be comparable to that of the parent strain (see Fig. S2 in the supplemental material). We then evaluated survival rates after lethal challenge over a 2-week period. The survival rate of the cCHP-PspA-vaccinated group was 100%, as was that for PspA-CT-vaccinated mice (Fig. 1). In contrast, most of the mice intranasally immunized with PspA alone (survival rate, 0%) or with PBS (20% survival) died within 8 days of challenge with *S. pneumoniae* Xen10 (Fig. 1). The survival rates of the groups immunized with cCHP-PspA or PspA-CT were higher and were statistically significant compared to that of the group immunized with PspA alone ($P < 0.01$). The results from the PspA-only and PBS-only groups did not differ ($P > 0.05$). In addition, immunization with the irrelevant antigen BoHc/A incorporated into cCHP (cCHP-BoHc/A) (35) did not protect mice from challenge with *S. pneumoniae* Xen10 (see Fig. S3). Because PspA family 2 (clades 3 through 5) and family 1 (clades 1 and 2) constitute 94 to 99% of clinical isolates of pneumococci (14, 44–49), we also challenged mice with the strain 3JYP3670, which expresses PspA belonging to clade 4 of family 2 (10). Unlike mice inoculated with cCHP-BoHc/A, PspA alone, or PBS only, mice nasally immunized with cCHP-PspA were protected from lethal challenge with 3JYP3670 (PspA of clade 4) (10), as was the case with Xen10 expressing PspA of clades 1 and 2 (see Fig. S4).

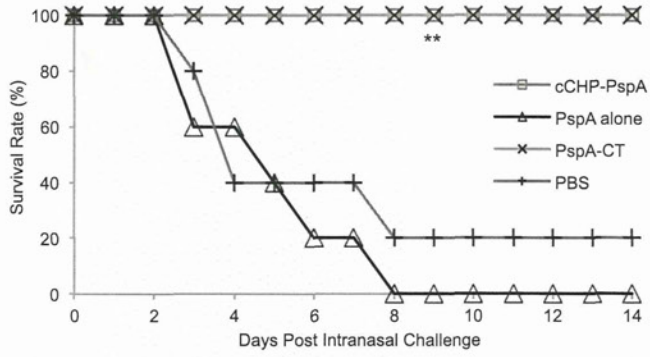

FIG 1 Intranasal vaccination with cCHP-PspA induced protective immunity against pneumococci. One week after the final immunization, mice were challenged with *S. pneumoniae* Xen10 (2×10^5 CFU/mouse), and survival was monitored. Data are representative of three independent experiments, and each group consisted of 5 mice. *P* values were calculated by using the Fisher exact test to compare the numbers of alive versus dead mice in each group with the result obtained for the PspA-only group. **, $P < 0.01$ compared with the group immunized with PspA alone. Abbreviations: cCHP, cationic cholesteryl group-bearing pullulan; CT, cholera toxin; PspA, pneumococcal surface protein A.

Intranasal vaccination with cCHP-PspA enhances bacterial clearance from BALF and the lung. To assess whether intranasal immunization with cCHP-PspA prevented pulmonary infection with pneumococci, we performed *in vivo* bioluminescence imaging of *S. pneumoniae* Xen10 after lethal challenge (2×10^5 CFU) of mice intranasally vaccinated with cCHP-PspA, PspA alone, or PBS. The lungs of mice immunized with PspA alone or with PBS only (control group) showed high-intensity photon signals in a pattern consistent with that of full-blown lung infection (Fig. 2A). In contrast, the lungs of mice immunized with cCHP-PspA lacked bioluminescence, indicating the absence of pulmonary infection. Forty-eight and 72 h after infection, photon counts of the cCHP-PspA-vaccinated group were significantly lower than those of the other two groups (Fig. 2B).

To investigate whether intranasal immunization with cCHP-PspA hastened bacterial clearance from the lung, we counted the bacteria in the BALF and lung tissues of mice intranasally vaccinated with cCHP-PspA, PspA alone, or PBS and sublethally challenged with *S. pneumoniae* Xen10 (2×10^4 CFU). Three hours after challenge, bacterial numbers in BALF (Fig. 2C) and lung tissue (Fig. 2D) did not differ among the three vaccination groups. However, 24 h after challenge, the bacterial counts in the BALF and lung homogenates from the cCHP-PspA-vaccinated groups were significantly lower (about 100-fold) than those for the mice immunized with PspA alone or PBS only (Fig. 2C and D).

Intranasal vaccination with cCHP-PspA reduces bacterial colonization in the nasal cavity. We next examined whether intranasal cCHP-PspA immunization affected nasal carriage of pneumococci in mice challenged with *S. pneumoniae* Xen10. Three days after challenge, bacterial numbers in NWs (Fig. 3A) and nasal passages (Fig. 3B) of mice immunized with the cCHP-PspA nasal vaccine were decreased significantly (approximately 100-fold) compared to those for the two control groups.

Intranasal vaccination with cCHP-PspA induces strong Th17 and Th2 responses. We then examined the type of immune

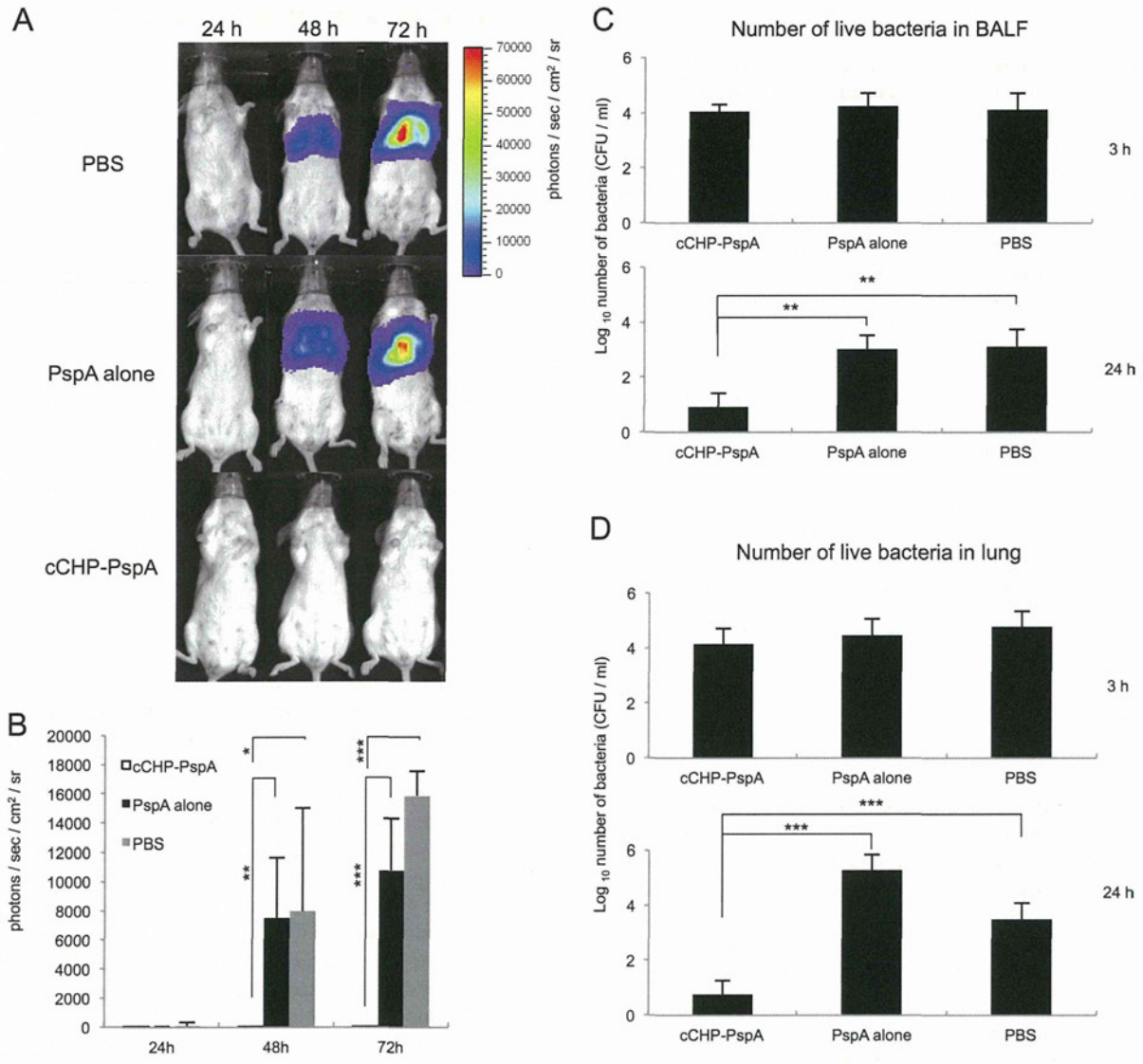

FIG 2 *In vivo* imaging revealed no sign of pneumococcal infection in the lungs of mice immunized intranasally with cCHP-PspA; these mice also showed enhanced bacterial clearance from the BALF and lung. Images (A) and average photon counts (B) show bioluminescence due to *S. pneumoniae* Xen10 in each group of mice infected intranasally with *S. pneumoniae* Xen10 (2×10^5 CFU/mouse) and imaged 24, 48, and 72 h after infection. (C and D) One week after the final immunization, mice were challenged with a sublethal dose (2×10^4 CFU/mouse) of *S. pneumoniae* Xen10. BALF and lung tissues were collected, and the numbers of *S. pneumoniae* Xen10 organisms 3 and 24 h after challenge were determined. Data are representative of three independent experiments, and each group consisted of 5 mice. *, $P < 0.05$; **, $P < 0.01$; ***, $P < 0.001$. Abbreviations: BALF, bronchoalveolar lavage fluid; cCHP, cationic cholesteryl-group-bearing pullulan; PspA, pneumococcal surface protein A.

responses elicited by intranasal cCHP-PspA vaccination. Compared with PspA alone or PBS, cCHP-PspA induced higher levels of IL-17 in $CD4^+$ T cells from the spleen, CLNs, and nasal passages (Fig. 4A). The cCHP-PspA-vaccinated group produced high levels of IL-4 and IL-13, the hallmark cytokines of a Th2-type immune response, but only scant amounts of gamma interferon (Fig. 4B to D). These results show the potential of a cCHP-PspA nasal vaccine as an advanced pneumococcal vaccine that can induce a Th17 response together with a Th2-type immune response.

Intranasal vaccination with cCHP-PspA induces high levels of systemic antibodies. To address whether intranasal administration of cCHP-PspA induced PspA-specific antibody responses, we examined the serum titers of PspA-specific antibodies. PspA-specific IgG responses in the systemic compartment were significantly higher in mice immunized with intranasal cCHP-PspA than in those given PspA only (Fig. 5A). Unlike the predominant IgG response, IgM and IgA titers in the serum samples were very low (Fig. 5A).

Intranasal immunization with cCHP-PspA induced primarily IgG1 antibodies, followed by IgG2b antibodies (Fig. 5B). This pattern indicated skewing toward a Th2-type response and was consistent with the cytokine profiles of the culture supernatants from antigen-stimulated $CD4^+$ T cells prepared from the same mice (Fig. 4B and C).

Intranasal vaccination with cCHP-PspA induces high levels of mucosal antigen-specific sIgA antibodies. We next examined whether vaccinated mice also produced mucosal antigen-specific Ig responses. Intranasal vaccination with cCHP-PspA induced

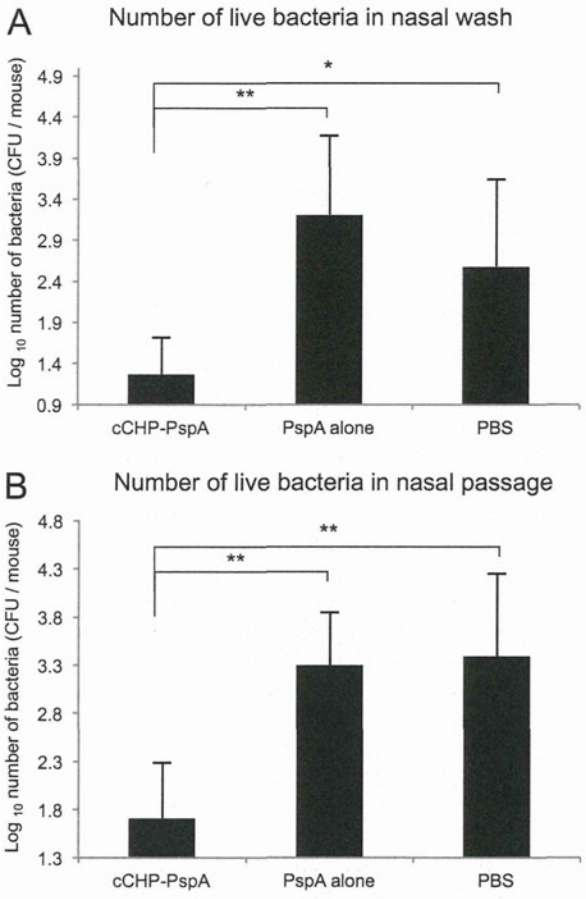

FIG 3 Intranasal vaccination with cCHP-PspA reduced bacterial colonization of the nasal cavity. One week after the final immunization, mice were challenged with a sublethal dose (2×10^4 CFU/mouse) of *Streptococcus pneumoniae* Xen10. Nasal washes and tissues were collected, and the numbers of *S. pneumoniae* Xen10 3 days after infection were determined. Data are representative of three independent experiments, and each group consisted of 5 mice. *, $P < 0.05$; **, $P < 0.01$. Abbreviations: cCHP, cationic cholesteryl group-bearing pullulan; PspA, pneumococcal surface protein A.

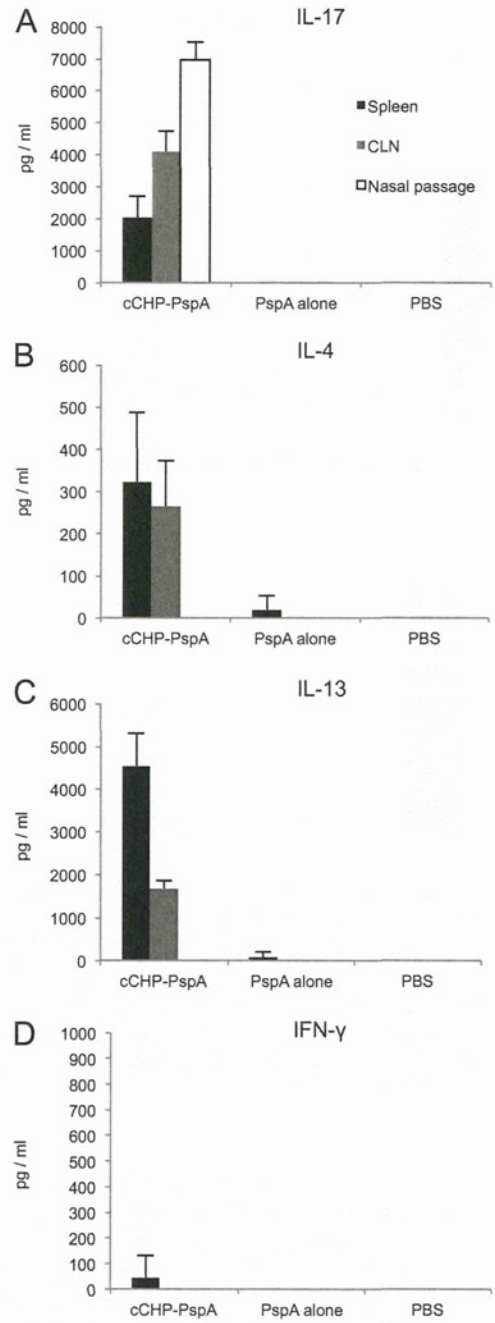

FIG 4 $CD4^+$ T cells from cCHP-PspA-immunized mice produce Th17- and Th2-type immune responses. Cytokines produced by $CD4^+$ T cells isolated from the spleens, cervical lymph nodes, and nasal passages of mice immunized with cCHP-PspA, PspA alone, or PBS only were analyzed. Data are representative of five independent experiments, and each group consisted of 5 mice. Abbreviations: cCHP, cationic cholesteryl-group-bearing pullulan; CLN, cervical lymph node; IFN-γ, gamma interferon; IL, interleukin; PspA, pneumococcal surface protein A.

PspA-specific mucosal IgA antibodies in the nasal secretions (Fig. 6A). In addition, BALF samples from mice intranasally vaccinated with cCHP-PspA contained PspA-specific IgA antibodies (Fig. 6B), and PspA-specific IgG antibodies were detected at high titers in both the NWs and BALF of mice intranasally immunized with cCHP-PspA (Fig. 6C and D). The nasal and BALF antigen-specific IgGs induced by intranasal immunization with cCHP-PspA were primarily of the IgG1 and IgG2b subclasses (Fig. 6E and F), similar to the Ig responses in the systemic compartment (Fig. 5B). Taken together, these results further support the benefit of cCHP-based nanogel as an effective nasal vaccine delivery vehicle for the induction of PspA-specific systemic and mucosal antibody responses against *S. pneumoniae*.

cCHP delivers PspA to dendritic cells (DCs) without CNS accumulation of PspA. The potential for antigen deposition and accumulation in the CNS through the olfactory fossa is one of the great concerns surrounding the use of nasal vaccines (33, 34, 50). To address this important concern, we instilled ^{111}In-labeled PspA alone or in complex with cCHP into the nasal cavities of mice. Beginning 6 h after administration, the nasal passages of mice treated with ^{111}In-labeled cCHP-PspA had higher SUVs than did those of mice treated with ^{111}In-labeled PspA alone, but there was no accumulation of ^{111}In-labeled PspA in the olfactory bulbs or brain throughout the 48-h observation period (Fig. 7A).

The cCHP vaccine delivery system enabled prolonged antigen exposure at the nasal epithelium, allowing continuous antigen

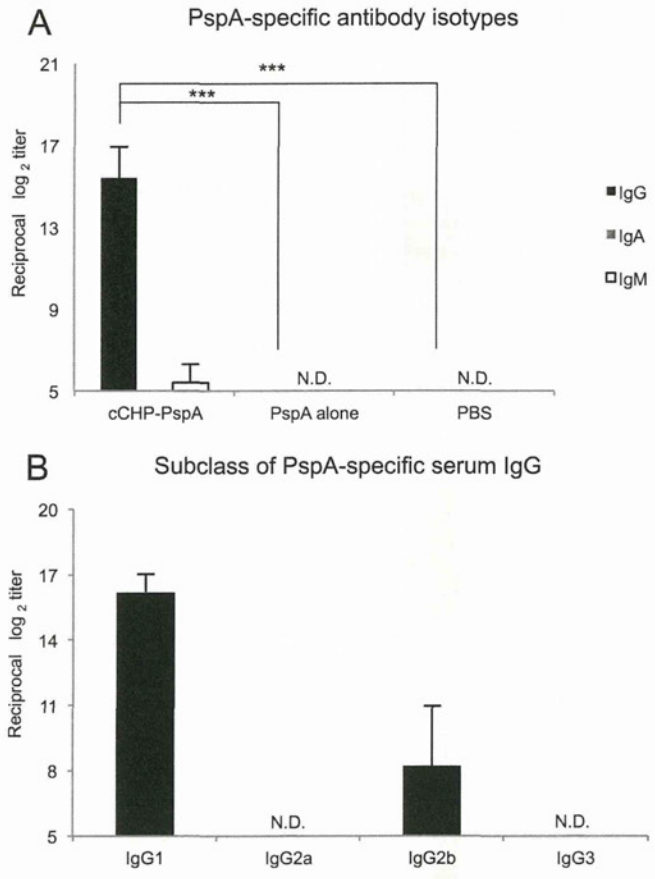

FIG 5 Intranasal vaccination with cCHP-PspA induced high levels of systemic antibodies. The data show the PspA-specific serum IgG level (A) and subclass analysis for IgG1, IgG2a, IgG2b, and IgG3 (B) for each immunized group (cCHP-PspA, PspA alone, or PBS only). Titers of PspA-specific IgG in sera were measured on day 7 after final immunization. Data are representative of three independent experiments, and each group consisted of 5 mice. N.D., not detected by ELISA with samples diluted 1:32. ***, $P < 0.001$. Abbreviations: cCHP, cationic cholesteryl group-bearing pullulan; Ig, immunoglobulin; PspA, pneumococcal surface protein A.

uptake by nasal DCs located in the epithelial layer and lamina propria of the nasal passages for the initiation of antigen-specific immune responses. Whereas 17.8% of the DCs located in the nasal passages had taken up PspA in the mice intranasally immunized with cCHP-PspA, only 0.7% of nasal DCs contained PspA antigen in mice that had been immunized intranasally with PspA alone (Fig. 7B). These results further support the concept that the cCHP-PspA vaccine formulation is an attractive inhalant delivery vehicle that effectively delivers and sustains antigen at the nasal epithelium for continuous antigen uptake by DCs without antigen deposition in the CNS.

DISCUSSION

We showed that cCHP-PspA-vaccinated mice survived a lethal challenge with *S. pneumoniae* (Fig. 1; see Fig. S4 in the supplemental material), whereas mice vaccinated with cCHP complexed with an irrelevant antigen (BoHc/A) did not (see Fig. S3 and S4). Importantly, compared with those of mice inoculated with control constructs, the respiratory tracts of mice immunized with intranasal cCHP-PspA had less colonization and invasion by pneumococcal organisms (Fig. 2 and 3). Intranasal administration of cCHP-PspA resulted in enhanced PspA-specific Th17 responses (Fig. 4A) and mucosal IgA and systemic IgG antibody responses (Fig. 5 and 6), all of which are involved in establishing protective immunity against pneumococci (10, 28–30). To our knowledge, the current study is the first to show the efficacy of a nasal vaccine not only for inducing protective immune responses but also for preventing nasal colonization by use of a single protein antigen (PspA) without adding any biologically active adjuvant.

The precise mechanisms underlying the efficacy of cCHP-PspA as a nasal vaccine against *S. pneumoniae* lung infection remain to be elucidated. However, we speculate that serum and BALF IgGs, the main isotype of antibody induced by the cCHP-PspA nasal vaccine in the lower respiratory compartment (Fig. 5A and 6D), play key roles in survival against lethal challenge with *S. pneumoniae*, given that antibody titers of PspA-specific IgA in the BALF were low (Fig. 6B) and therefore might contribute only minimally to protection against invasive diseases. This hypothesis is supported by the results of a previous study (28) in which $IgA^{-/-}$ mice immunized with intranasal PspA-adjuvant (i.e., a plasmid expressing Flt3 ligand cDNA) mounted a protective immune response against lethal challenge with *S. pneumoniae*. Our current study shows that the cCHP-PspA nasal vaccine effectively induced antigen-specific sIgA antibodies in the upper airways (Fig. 6A). Immunization of $IgA^{-/-}$ mice with intranasal PspA-adjuvant did not prevent pneumococcal colonization of the nasal cavity (28). In light of the findings of the previous study (28) and our current one, serum antigen-specific IgG antibodies are crucial to preventing invasive disease associated with clinical signs, whereas antigen-specific sIgA antibodies are essential for preventing colonization of the upper respiratory tract by *S. pneumoniae*.

In addition to the essential role of sIgA in protection from nasopharyngeal colonization by pneumococci, IL-17A-producing $CD4^+$ T cells play an important role in preventing pneumococcal nasal colonization in mice immunized with intranasal pneumococcal whole-cell antigen (29, 30). Recent studies have found that IL-17 promotes multiple aspects of humoral immunity by enhancing B cell proliferation and isotype switching (51), B cell recruitment to the respiratory mucosa, and expression of the polymeric immunoglobulin receptor on the airway epithelium (52). In the current study, we found that intranasal immunization with cCHP-PspA generated Th17 cells in the nasal passages, draining lymph nodes, and systemic compartment (Fig. 4A). Therefore, our findings suggest that intranasal immunization with cCHP-PspA induces both humoral and cellular immune responses, which are required for protective immunity against pneumococcal colonization and invasive disease. In addition to their essential role in antipneumococcal immunity (29, 30), Th17 responses are a hallmark of autoimmunity (53). Therefore, future studies should carefully examine whether the Th17 responses induced by intranasal immunization with cCHP-PspA are associated with any adverse effects.

As one might expect, the protective immunity induced by nasal cCHP-PspA was not observed when an irrelevant antigen, BoHc/A, was incorporated into cCHP (cCHP-BoHc/A) (35) and used as a nasal vaccine (see Fig. S3 and S4 in the supplemental material). Moreover, mice immunized intranasally with cCHP-PspA (PspA of clades 1 and 2) were protected against challenge with pneumococcal strain 3JYP3670, which expresses PspA of clade 4 (10), whereas mice immunized with cCHP-BoHc/A, PspA

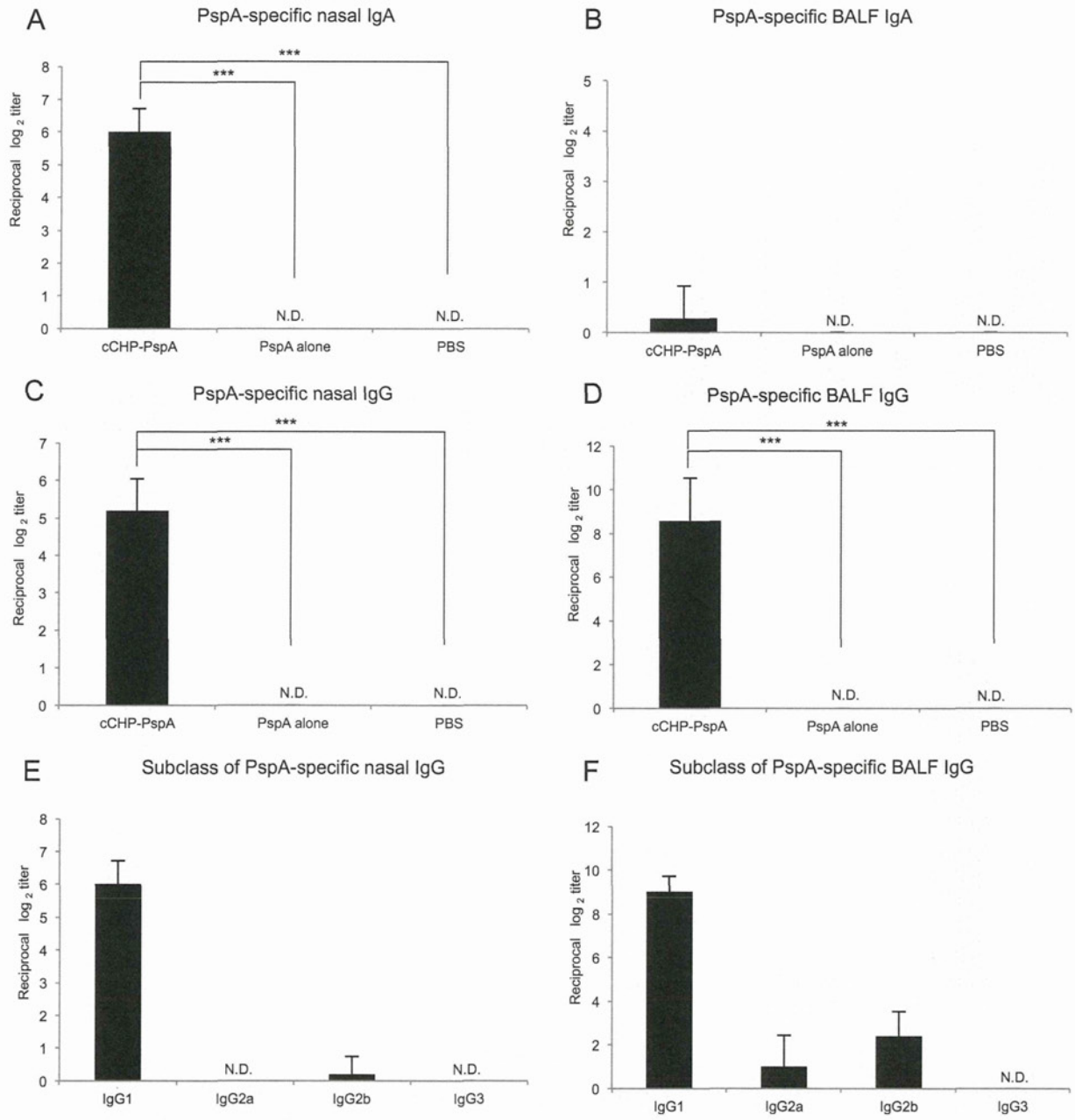

FIG 6 Intranasal vaccination with cCHP-PspA induced strong PspA-specific secretory IgA and IgG responses. Titers of nasal (A and C) and bronchial (B and D) IgA and IgG induced by intranasal immunization with PspA alone or PspA mixed with cCHP are shown. Titers of PspA-specific IgA and IgG in nasal washes and BALFs were measured on day 7 after final immunization. Intranasal cCHP-PspA vaccination induced high levels of IgG1 and IgG2b in mucosal secretions of the upper (E) and lower (F) airways. Data are representative of five independent experiments, and each group consisted of 5 mice. N.D., not detected in undiluted samples. ***, $P < 0.001$. Abbreviations: BALF, bronchoalveolar lavage fluid; cCHP, cationic cholesteryl-group-bearing pullulan; Ig, immunoglobulin; PspA, pneumococcal surface protein A.

alone, or PBS were not (see Fig. S4). These findings highlight the potential advantage of nasal vaccination of cCHP-PspA in inducing antigen-specific protective immunity with subtype cross-reactivity.

Note that cCHP lacks any biologically active adjuvant effect because it cannot activate immune cells by itself (35). The nanogel formulation had no effect on the expression of costimulatory molecules on nasal DCs (see Fig. S5 in the supplemental material), which are supposed to already express high steady-state levels of costimulatory molecules in the mucosal environment in response to numerous inhaled antigens. Our current and previous studies have shown that antigens are released from the nanogel and are taken up efficiently by DCs in the nasal mucosa (Fig. 7B) (35). These studies suggest that cCHP nanogel is an effective carrier that has strong chaperone-like activity, enabling the delivery of PspA across the nasal mucosal epithelial cell layer for subsequent uptake by DCs and initiation of antigen-specific immune responses.

In summary, this study introduced a promising nanometer-

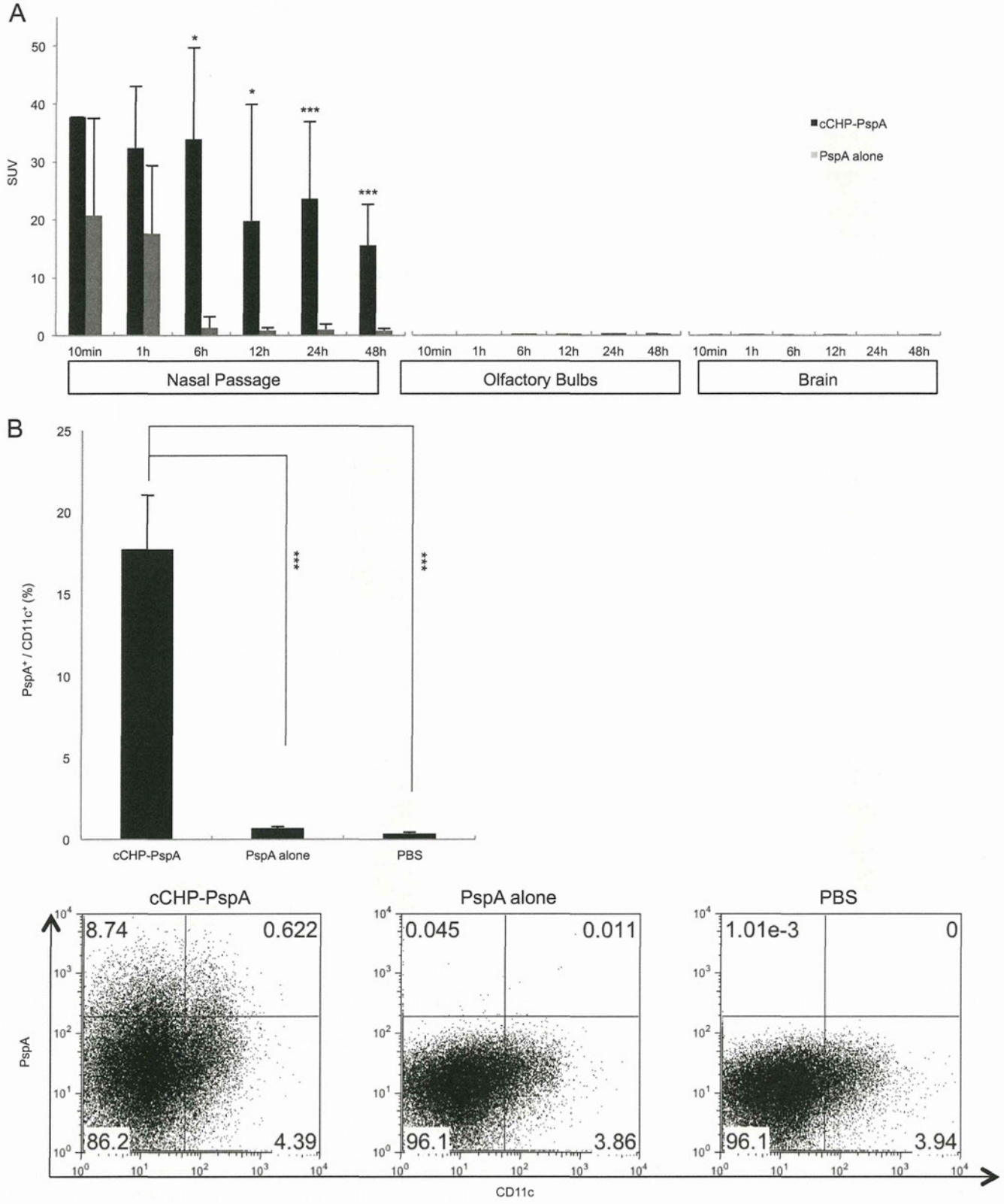

FIG 7 Intranasal vaccination with cCHP-PspA induced no accumulation of PspA in the central nervous system (A) but enhanced the efficiency of uptake of PspA by dendritic cells in the nasal passages (B). (A) ^{111}In-labeled PspA was administered intranasally with or without cCHP nanogel, and the radioisotope counts (SUVs) in the nasal passages, olfactory bulbs, and brain were estimated 10 min and 1, 6, 12, 24, and 48 h after instillation. (B) Dendritic cells in the nasal passages of mice immunized intranasally with cCHP-PspA, PspA alone, or PBS were analyzed by flow cytometry 6 h after immunization. Data are representative of three independent experiments, and each group consisted of 5 mice. *, $P < 0.05$; ***, $P < 0.001$. Abbreviations: cCHP, cationic cholesteryl group-bearing pullulan; PspA, pneumococcal surface protein A.

sized carrier-based pneumococcal nasal vaccine that incorporates cCHP nanogel and the pneumococcal serotype-independent protein antigen PspA. The antigen-specific immune responses induced by this vaccine effectively protected mice against the respiratory pathogen *S. pneumoniae*. Our results confirmed that cCHP nanogel is a promising candidate carrier of a protein antigen for a mucosal vaccine that induces humoral and cellular immune responses against PspA to combat colonization and invasion of the airways by respiratory pathogens.

ACKNOWLEDGMENTS

This study was supported by a grant-in-aid from the Research Fellowship of the Japan Society for the Promotion of Science (JSPS) (I.G.K., A.S., and T.N.); by programs of special coordination funds for promoting science and technology, a grant-in-aid for scientific research on priority areas, and a grant-in-aid for scientific research from the Ministry of Education, Culture, Sports, Science, and Technology of Japan (J.K. and H.K.); by the Ministry of Health, Labor, and Welfare of Japan (J.K., Y.Y., and H.K.); by the New Energy and Industrial Technology Development Organization (NEDO) (Y.Y. and H.K.); by the Young Researcher Overseas Visits Program for Vitalizing Brain Circulation of the Japan Society for the Promotion of Science (J.K., H.K., and Y.Y.); by the Program for Promotion of Basic and Applied Researches for Innovations in Bio-Oriented Industry (BRAIN) (T.N., S. Sato, and J.K.); by the Yakult Bio-Science Foundation (J.K.); and by the Global Center of Excellence Program "Center of Education and Research for Advanced Genome-Based Medicine—For Personalized Medicine and the Control of Worldwide Infectious Diseases" (H.K.).

We declare that we have no conflicts of interest.

REFERENCES

1. **Dinleyici EC, Yargic ZA.** 2008. Pneumococcal conjugated vaccines: impact of PCV-7 and new achievements in the postvaccine era. Expert Rev. Vaccines 7:1367–1394.
2. **Rose M, Zielen S.** 2009. Impact of infant immunization programs with pneumococcal conjugate vaccine in Europe. Expert Rev. Vaccines **8**:1351–1364.
3. **Principi N, Esposito S.** 2012. Use of the 13-valent pneumococcal conjugate vaccine in infants and young children. Expert Opin. Biol. Ther. **12**: 641–648.
4. **Huang SS, Johnson KM, Ray GT, Wroe P, Lieu TA, Moore MR, Zell ER, Linder JA, Grijalva CG, Metlay JP, Finkelstein JA.** 2011. Healthcare utilization and cost of pneumococcal disease in the United States. Vaccine **29**:3398–3412.
5. **Thigpen MC, Whitney CG, Messonnier NE, Zell ER, Lynfield R, Hadler JL, Harrison LH, Farley MM, Reingold A, Bennett NM, Craig AS, Schaffner W, Thomas A, Lewis MM, Scallan E, Schuchat A.** 2011. Bacterial meningitis in the United States, 1998–2007. N. Engl. J. Med. **364**:2016–2025.
6. **Weinberger DM, Malley R, Lipsitch M.** 2011. Serotype replacement in disease after pneumococcal vaccination. Lancet **378**:1962–1973.
7. **Hsu HE, Shutt KA, Moore MR, Beall BW, Bennett NM, Craig AS, Farley MM, Jorgensen JH, Lexau CA, Petit S, Reingold A, Schaffner W, Thomas A, Whitney CG, Harrison LH.** 2009. Effect of pneumococcal conjugate vaccine on pneumococcal meningitis. N. Engl. J. Med. **360**: 244–256.
8. **Singleton RJ, Hennessy TW, Bulkow LR, Hammitt LL, Zulz T, Hurlburt DA, Butler JC, Rudolph K, Parkinson A.** 2007. Invasive pneumococcal disease caused by nonvaccine serotypes among Alaska native children with high levels of 7-valent pneumococcal conjugate vaccine coverage. JAMA **297**:1784–1792.
9. **Briles DE, Hollingshead SK, Nabors GS, Paton JC, Brooks-Walter A.** 2000. The potential for using protein vaccines to protect against otitis media caused by *Streptococcus pneumoniae*. Vaccine **19**(Suppl 1):S87–S95.
10. **Briles DE, Hollingshead SK, King J, Swift A, Braun PA, Park MK, Ferguson LM, Nahm MH, Nabors GS.** 2000. Immunization of humans with recombinant pneumococcal surface protein A (rPspA) elicits antibodies that passively protect mice from fatal infection with *Streptococcus pneumoniae* bearing heterologous PspA. J. Infect. Dis. **182**:1694–1701.
11. **Briles DE, Hollingshead SK, Paton JC, Ades EW, Novak L, van Ginkel FW, Benjamin Jr, WH.** 2003. Immunizations with pneumococcal surface protein A and pneumolysin are protective against pneumonia in a murine model of pulmonary infection with *Streptococcus pneumoniae*. J. Infect. Dis. **188**:339–348.
12. **Briles DE, Tart RC, Swiatlo E, Dillard JP, Smith P, Benton KA, Ralph BA, Brooks-Walter A, Crain MJ, Hollingshead SK, McDaniel LS.** 1998. Pneumococcal diversity: considerations for new vaccine strategies with emphasis on pneumococcal surface protein A (PspA). Clin. Microbiol. Rev. **11**:645–657.
13. **Olafsdottir TA, Lingnau K, Nagy E, Jonsdottir I.** 2012. Novel protein-based pneumococcal vaccines administered with the Th1-promoting adjuvant IC31 induce protective immunity against pneumococcal disease in neonatal mice. Infect. Immun. **80**:461–468.
14. **Hollingshead SK, Becker R, Briles DE.** 2000. Diversity of PspA: mosaic genes and evidence for past recombination in *Streptococcus pneumoniae*. Infect. Immun. **68**:5889–5900.
15. **Crain MJ, Waltman WD, 2nd, Turner JS, Yother J, Talkington DF, McDaniel LS, Gray BM, Briles DE.** 1990. Pneumococcal surface protein A (PspA) is serologically highly variable and is expressed by all clinically important capsular serotypes of *Streptococcus pneumoniae*. Infect. Immun. **58**:3293–3299.
16. **McDaniel LS, Sheffield JS, Delucchi P, Briles DE.** 1991. PspA, a surface protein of *Streptococcus pneumoniae*, is capable of eliciting protection against pneumococci of more than one capsular type. Infect. Immun. **59**:222–228.
17. **Tart RC, McDaniel LS, Ralph BA, Briles DE.** 1996. Truncated *Streptococcus pneumoniae* PspA molecules elicit cross-protective immunity against pneumococcal challenge in mice. J. Infect. Dis. **173**:380–386.
18. **Xin W, Li Y, Mo H, Roland KL, Curtiss R.** 2009. PspA family fusion proteins delivered by attenuated *Salmonella enterica* serovar Typhimurium extend and enhance protection against *Streptococcus pneumoniae*. Infect. Immun. **77**:4518–4528.
19. **Nabors GS, Braun PA, Herrmann DJ, Heise ML, Pyle DJ, Gravenstein S, Schilling M, Ferguson LM, Hollingshead SK, Briles DE, Becker RS.** 2000. Immunization of healthy adults with a single recombinant pneumococcal surface protein A (PspA) variant stimulates broadly cross-reactive antibodies to heterologous PspA molecules. Vaccine **18**:1743–1754.
20. **Gray BM, Converse GM, 3rd, Dillon HC, Jr.** 1980. Epidemiologic studies of *Streptococcus pneumoniae* in infants: acquisition, carriage, and infection during the first 24 months of life. J. Infect. Dis. **142**:923–933.
21. **Faden H, Duffy L, Wasielewski R, Wolf J, Krystofik D, Tung Y.** 1997. Relationship between nasopharyngeal colonization and the development of otitis media in children. J. Infect. Dis. **175**:1440–1445.
22. **Leiberman A, Dagan R, Leibovitz E, Yagupsky P, Fliss DM.** 1999. The bacteriology of the nasopharynx in childhood. Int. J. Pediatr. Otorhinolaryngol. **49**(Suppl 1):S151–S153.
23. **Hoge CW, Reichler MR, Dominguez EA, Bremer JC, Mastro TD, Hendricks KA, Musher DM, Elliott JA, Facklam RR, Breiman RF.** 1994. An epidemic of pneumococcal disease in an overcrowded, inadequately ventilated jail. N. Engl. J. Med. **331**:643–648.
24. **Wu HY, Nahm MH, Guo Y, Russell MW, Briles DE.** 1997. Intranasal immunization of mice with PspA (pneumococcal surface protein A) can prevent intranasal carriage, pulmonary infection, and sepsis with *Streptococcus pneumoniae*. J. Infect. Dis. **175**:839–846.
25. **Yamamoto M, Briles DE, Yamamoto S, Ohmura M, Kiyono H, McGhee JR.** 1998. A nontoxic adjuvant for mucosal immunity to pneumococcal surface protein A. J. Immunol. **161**:4115–4121.
26. **Briles DE, Ades E, Paton JC, Sampson JS, Carlone GM, Huebner RC, Virolainen A, Swiatlo E, Hollingshead SK.** 2000. Intranasal immunization of mice with a mixture of the pneumococcal proteins PsaA and PspA is highly protective against nasopharyngeal carriage of *Streptococcus pneumoniae*. Infect. Immun. **68**:796–800.
27. **Oma K, Zhao J, Ezoe H, Akeda Y, Koyama S, Ishii KJ, Kataoka K, Oishi K.** 2009. Intranasal immunization with a mixture of PspA and a Toll-like receptor agonist induces specific antibodies and enhances bacterial clearance in the airways of mice. Vaccine **27**:3181–3188.
28. **Fukuyama Y, King JD, Kataoka K, Kobayashi R, Gilbert RS, Oishi K, Hollingshead SK, Briles DE, Fujihashi K.** 2010. Secretory-IgA antibodies play an important role in the immunity to *Streptococcus pneumoniae*. J. Immunol. **185**:1755–1762.
29. **Lu YJ, Gross J, Bogaert D, Finn A, Bagrade L, Zhang Q, Kolls JK, Srivastava A, Lundgren A, Forte S, Thompson CM, Harney KF, An-**

derson PW, Lipsitch M, Malley R. 2008. Interleukin-17A mediates acquired immunity to pneumococcal colonization. PLoS Pathog. 4:e1000159. doi:10.1371/journal.ppat.1000159.
30. Malley R. 2005. $CD4^+$ T cells mediate antibody-independent acquired immunity to pneumococcal colonization. Proc. Natl. Acad. Sci. U. S. A. 102:4848–4853.
31. Xu-Amano J, Kiyono H, Jackson RJ, Staats HF, Fujihashi K, Burrows PD, Elson CO, Pillai S, McGhee JR. 1993. Helper T cell subsets for immunoglobulin A responses: oral immunization with tetanus toxoid and cholera toxin as adjuvant selectively induces Th2 cells in mucosa associated tissues. J. Exp. Med. 178:1309–1320.
32. Freytag LC, Clements JD. 2005. Mucosal adjuvants. Vaccine 23:1804–1813.
33. Mutsch M, Zhou W, Rhodes P, Bopp M, Chen RT, Linder T, Spyr C, Steffen R. 2004. Use of the inactivated intranasal influenza vaccine and the risk of Bell's palsy in Switzerland. N. Engl. J. Med. 350:896–903.
34. van Ginkel FW, Jackson RJ, Yuki Y, McGhee JR. 2000. Cutting edge: the mucosal adjuvant cholera toxin redirects vaccine proteins into olfactory tissues. J. Immunol. 165:4778–4782.
35. Nochi T, Yuki Y, Takahashi H, Sawada S, Mejima M, Kohda T, Harada N, Kong IG, Sato A, Kataoka N, Tokuhara D, Kurokawa S, Takahashi Y, Tsukada H, Kozaki S, Akiyoshi K, Kiyono H. 2010. Nanogel antigenic protein-delivery system for adjuvant-free intranasal vaccines. Nat. Mater. 9:572–578.
36. Reference deleted.
37. Ayame H, Morimoto N, Akiyoshi K. 2008. Self-assembled cationic nanogels for intracellular protein delivery. Bioconjug. Chem. 19:882–890.
38. Kurono Y, Yamamoto M, Fujihashi K, Kodama S, Suzuki M, Mogi G, McGhee JR, Kiyono H. 1999. Nasal immunization induces *Haemophilus influenzae*-specific Th1 and Th2 responses with mucosal IgA and systemic IgG antibodies for protective immunity. J. Infect. Dis. 180:122–132.
39. Darrieux M, Miyaji EN, Ferreira DM, Lopes LM, Lopes AP, Ren B, Briles DE, Hollingshead SK, Leite LC. 2007. Fusion proteins containing family 1 and family 2 PspA fragments elicit protection against *Streptococcus pneumoniae* that correlates with antibody-mediated enhancement of complement deposition. Infect. Immun. 75:5930–5938.
40. Francis KP, Yu J, Bellinger-Kawahara C, Joh D, Hawkinson MJ, Xiao G, Purchio TF, M. Caparon G, Lipsitch M, Contag PR. 2001. Visualizing pneumococcal infections in the lungs of live mice using bioluminescent *Streptococcus pneumoniae* transformed with a novel gram-positive *lux* transposon. Infect. Immun. 69:3350–3358.
41. Kadurugamuwa JL, Modi K, Coquoz O, Rice B, Smith S, Contag PR, Purchio T. 2005. Reduction of astrogliosis by early treatment of pneumococcal meningitis measured by simultaneous imaging, in vivo, of the pathogen and host response. Infect. Immun. 73:7836–7843.
42. Michel RB, Andrews PM, Castillo ME, Mattes MJ. 2005. *In vitro* cytotoxicity of carcinoma cells with ^{111}In-labeled antibodies to HER-2. Mol. Cancer Ther. 4:927–937.
43. Fukuyama S, Hiroi T, Yokota Y, Rennert PD, Yanagita M, Kinoshita N, Terawaki S, Shikina T, Yamamoto M, Kurono Y, Kiyono H. 2002. Initiation of NALT organogenesis is independent of the IL-7R, LTβR, and NIK signaling pathways but requires the Id2 gene and $CD3^-CD4^+CD45^+$ cells. Immunity 17:31–40.
44. Hollingshead SK. 2006. Pneumococcal surface protein A (PspA) family distribution among clinical isolates from adults over 50 years of age collected in seven countries. J. Med. Microbiol. 55:215–221.
45. Ren B, Szalai AJ, Hollingshead SK, Briles DE. 2004. Effects of PspA and antibodies to PspA on activation and deposition of complement on the pneumococcal surface. Infect. Immun. 72:114–122.
46. Beall B, Gherardi G, Facklam RR, Hollingshead SK. 2000. Pneumococcal PspA sequence types of prevalent multiresistant pneumococcal strains in the United States and of internationally disseminated clones. J. Clin. Microbiol. 38:3663–3669.
47. Brandileone M. 2004. Typing of pneumococcal surface protein A (PspA) in *Streptococcus pneumoniae* isolated during epidemiological surveillance in Brazil: towards novel pneumococcal protein vaccines. Vaccine 22:3890–3896.
48. Mollerach M, Regueira M, Bonofiglio L, Callejo R, Pace J, Di Fabio JL, Hollingshead SK, Briles DE. 2004. Invasive *Streptococcus pneumoniae* isolates from Argentinian children: serotypes, families of pneumococcal surface protein A (PspA) and genetic diversity. Epidemiol. Infect. 132:177–184.
49. Vela Coral MC, Fonseca N, Castaneda E, Di Fabio JL, Hollingshead SK, Briles DE. 2001. Pneumococcal surface protein A of invasive *Streptococcus pneumoniae* isolates from Colombian children. Emerg. Infect. Dis. 7:832–836.
50. Dubin PJ, Kolls JK. 2009. Interleukin-17A and interleukin-17F: a tale of two cytokines. Immunity 30:9–11.
51. Doreau A, Belot A, Bastid J, Riche B, Trescol-Biemont MC, Ranchin B, Fabien N, Cochat P, Pouteil-Noble C, Trolliet P, Durieu I, Tebib J, Kassai B, Ansieau S, Puisieux A, Eliaou JF, Bonnefoy-Berard N. 2009. Interleukin 17 acts in synergy with B cell-activating factor to influence B cell biology and the pathophysiology of systemic lupus erythematosus. Nat. Immunol. 10:778–785.
52. Jaffar Z, Ferrini ME, Herritt LA, Roberts K. 2009. Cutting edge: lung mucosal Th17-mediated responses induce polymeric Ig receptor expression by the airway epithelium and elevate secretory IgA levels. J. Immunol. 182:4507–4511.
53. Bettelli E, Oukka M, Kuchroo VK. 2007. Th17 cells in the circle of immunity and autoimmunity. Nat. Immunol. 8:345–350.

Transcription factor Spi-B–dependent and –independent pathways for the development of Peyer's patch M cells

S Sato[1,2], S Kaneto[1,3], N Shibata[1,4], Y Takahashi[1], H Okura[1,4], Y Yuki[1], J Kunisawa[1,4,5] and H Kiyono[1,2,3,4,6]

Although many of the biological features of microfold cells (M cells) have been known for many years, the molecular mechanisms of M-cell development and antigen recognition have remained unclear. Here, we report that *Umod* is a novel M-cell–specific gene, the translation products of which might contribute to the uptake function of M cells. Transcription factor Spi-B was also specifically expressed in M cells among non-hematopoietic lineages. Spi-B–deficient mice showed reduced expression of most, but not all, other M-cell–specific genes and M-cell surface markers. Whereas uptake of *Salmonella* Typhimurium via M cells was obviously reduced in Spi-B–deficient mice, the abundance of intratissue cohabiting bacteria was comparable between wild-type and Spi-B–deficient mice. These data indicate that there is a small M-cell population with developmental regulation that is Spi-B independent; however, Spi-B is probably a candidate master regulator of M-cell functional maturation and development by another pathway.

INTRODUCTION

Mucosa-associated lymphoid tissues, represented in the small intestine by Peyer's patches (PPs), are the inductive sites of the mucosal immune system.[1] Unlike other peripheral lymphoid tissues, mucosa-associated lymphoid tissues do not have afferent vessels; instead, they have a direct antigen-sampling system that takes antigens into the tissue from the mucosal surface. This antigen uptake is managed mainly by microfold cells (M cells), which are located within the follicle-associated epithelium (FAE) of mucosa-associated lymphoid tissues and are regarded as professional antigen-sampling cells.[1] M cells have unique morphological features, such as relatively short, irregular microvilli on their apical surfaces and a pocket structure on their basolateral side that enfolds lymphocytes and antigen-presenting cells. These distinctive features are considered to contribute to M-cell functions: the short microvilli enable easy contact with luminal antigens, and the ability to hold antigen-presenting cells, such as dendritic cells, in their pockets is valuable for the prompt transfer of antigens to dendritic cells for speedy initiation of antigen-specific mucosal immunity. Because M cells are principal targets for effective peroral vaccination, elucidation of the molecular mechanisms behind their antigen-uptake functions and differentiation is important for the development of new-era oral vaccines.

We have reported that glycoprotein 2 (GP2) is specifically expressed on M cells,[2] and a progressive study has demonstrated that GP2 acts as a binding receptor for FimH-expressing bacteria, inducing effective uptake of, and specific immune responses to, such bacteria.[3] Although several other M-cell–specific molecules, such as MARCKS-like protein,[2] peptidoglycan recognition protein S,[4] and fucosyltransferase 1 (FUT1),[5] have been reported, the functions of these molecules in contributing to antigen uptake have not yet been revealed. In addition, the mechanisms of M-cell differentiation are poorly understood.

Recently, it has been reported that the intestinal epithelial crypt–villus structure can be assembled from a single Lgr5-positive stem cell in the absence of a non-epithelial-cell niche.[6] It has also been reported that almost all small intestinal epithelial cell (EC) lineages develop from intestinal epithelial

[1]Division of Mucosal Immunology, Department of Microbiology and Immunology, The Institute of Medical Science, The University of Tokyo, Tokyo, Japan. [2]Core Research for Evolutional Science and Technology (CREST), Japan Science and Technology Agency, Tokyo, Japan. [3]Graduate School of Medicine, The University of Tokyo, Tokyo, Japan. [4]Department of Medical Genome Science, Graduate School of Frontier Science, The University of Tokyo, Chiba, Japan. [5]Laboratory of Vaccine Materials, National Institute of Biomedical Innovation, Osaka, Japan and [6]International Research and Development Center for Mucosal Vaccines, The Institute of Medical Science, The University of Tokyo, Tokyo, Japan. Correspondence: H Kiyono (kiyono@ims.u-tokyo.ac.jp)

Received 16 July 2012; accepted 1 November 2012; advance online publication 5 December 2012. doi:10.1038/mi.2012.122

stem cells. First, the expression of Math1 transcription factor determines the destiny of stem cells for the secretory lineage.[7] Further differentiation of secretory lineage cells, such as goblet cells, Paneth cells, and endocrine cells, requires other factors such as Klf4, Sox9, and Ngn3, respectively.[8–11] On the other hand, if the stem cells express Hes1, which inhibits Math1 expression, these cells adopt a non-secretory lineage and become, for example, enterocytes.[12] Because M cells belong to a non-secretory lineage, at least one unknown factor might be expressed and activated downstream of Hes1 in precursor cells for differentiation into M cells.

Here, we report the existence of two additional M-cell–specific genes among mouse intestinal ECs, as determined from the data obtained in our previously reported DNA gene chip analysis.[2] One is *Umod*, which encodes the cell-surface expression molecule Tamm–Horsfall protein (THP). The other one, *Spib*, encodes Spi-B, which is a transcription factor belonging to the Ets family. In focusing on the function of Spi-B, our investigations revealed that M-cell–intrinsic Spi-B controls the expression of other, but not all, M-cell–specific genes. In addition, Spi-B regulates the ultrastructural development and GP2-mediated antigen-uptake functions of most PP M cells, whereas a translocation of the majority of *Alcaligenes* spp., which are commensal bacteria resident in PPs and isolated lymphoid follicles preferentially through M cells, was observed independently of Spi-B. We propose that M-cell–intrinsic Spi-B is an essential transcription factor for the functional and structural differentiation of M cells, although a small population of M cells may mature independently of Spi-B. These M cells, which were found within the FAE of Spi-B–deficient mice, might still be present in sufficient numbers to contribute to the migration of mucosa-associated lymphoid tissue-resident bacteria.

RESULTS

Spib and *Umod* are expressed in M cells but not other intestinal ECs

We previously reported the discovery of a series of PP M-cell–specific genes by DNA gene chip analysis.[2] To search for other M-cell–specific molecules—especially a key transcription factor for M-cell development or function—we used real-time polymerase chain reaction (PCR) to screen candidate genes from gene chip analysis data. Whole ECs and lymphocytes were prepared from well-trimmed duodenal PPs as "PP ECs" and "PP lymphocytes," respectively. PP M cells and non-M cells were then purified from PP ECs as NKM 16-2-4 antibody (NKM)/*Ulex europaeus* agglutinin 1 (UEA-1) double-positive and double-negative cells, respectively.[13] Among several candidates, we confirmed that *Spib* and *Umod* were preferentially expressed in PP M cells (**Figure 1a**). We next performed an *in situ* hybridization analysis of *Spib* and *Umod* expressions in PPs to confirm the real-time PCR data. An antisense cRNA probe for *Spib* specifically stained part of the FAE region of the PP among the intestinal ECs (**Figure 1b**) and (as was expect from the previous studies[14,15]) in the lymphocyte region of the PPs, especially in the germinal centers (**Figure 1b,c**, dotted circles). Similarly, *Umod* expression was observed within the FAE region. A negative control experiment using each sense probe gave no signals for either *Spib* or *Umod*. In addition, expression of both *Spib* and *Umod* was well colocalized with UEA-1–positive cells (**Figure 1c**). These findings demonstrated that *Spib* and *Umod* were expressed in PP M cells but not in other intestinal ECs.

Expression of M-cell–specific surface markers is severely diminished in Spi-B–deficient mice

Expression of *Spib* in PP M cells was high—at levels comparable to that of *Gp2* and *Marcksl1*, which were previously reported to be M-cell–specific genes.[2] In addition, because Spi-B is a transcription factor belonging to the Ets family, it is probable that it controls the expression of genes encoding molecules that contribute to M-cell function or development, or both. Therefore, we decided to focus our efforts on investigating an *in vivo* role of Spi-B in M cells. Spi-B–deficient ($Spib^{-/-}$) mice[15] were thus employed and the characteristics of their PP M cells were compared with those of wild-type ($Spib^{+/+}$) mice.

GP2 is expressed on M cells and not on other intestinal ECs;[2,3] therefore, we first examined GP2 expression by using whole-mount staining. In wild-type mice, GP2 expression was clearly and specifically detected in the FAE region (**Figure 2a**), as demonstrated previously.[2,3] In contrast, $Spib^{-/-}$-derived PPs completely lost their GP2 expression, as found in $Gp2^{-/-}$-derived PPs[3] (**Figure 2b**). More classically, mouse PP M cells were defined as NKM antibody (and/or UEA-1)–positive and wheat germ agglutinin–negative ($NKM^{+}WGA^{-}$) FAE cells,[13] as seen in the PPs from $Spib^{+/+}$ mice (**Figure 2c**). $Spib^{-/-}$-derived PPs showed reduced numbers of $NKM^{+}WGA^{-}$ cells (**Figure 2d–f**); these cells are considered to have the hallmarks of M cells. Notably, although GP2-positive FAE cells were completely abolished in $Spib^{-/-}$ mice (**Figure 2b**), a few $NKM^{+}WGA^{-}$ cells were found in $Spib^{-/-}$-derived PPs (**Figure 2e,f**; about 10 per FAE region vs. about 350 per FAE region in the case of $Spib^{+/+}$ cells).

Gp2 is a target gene of Spi-B

Because GP2 is a highly glycosylated protein and the anti-mouse GP2 antibody used in this research (clone 2F11-C3) was raised against recombinant mouse GP2-Fc fusion protein produced by mammalian cells,[3] it was possible that recognition of GP2 by 2F11-C3 antibody depended on glycosylation. Hence, we next checked the expression level of *Gp2* transcript in the FAE region by using quantitative real-time PCR. Consistent with the whole-mount staining data, *Gp2* expression was dramatically suppressed in $Spib^{-/-}$ mice-derived FAE (**Figure 3a**), indicating that *Gp2* expression is exclusively regulated by Spi-B.

UEA-1 and NKM antibody recognize α (1,2)-fucose, which specifically binds the terminal galactose residues of some surface membrane proteins.[13] Given that terminal fucosylation on PP M cells is catalyzed by FUT1, which is coded by the M-cell–specific gene *Fut1* (Terahara *et al.*[5] and **Supplementary Figure S1** online), the cause of the decrease in numbers of $NKM^{+}WGA^{-}$ cells in the FAE of $Spib^{-/-}$ mice might have

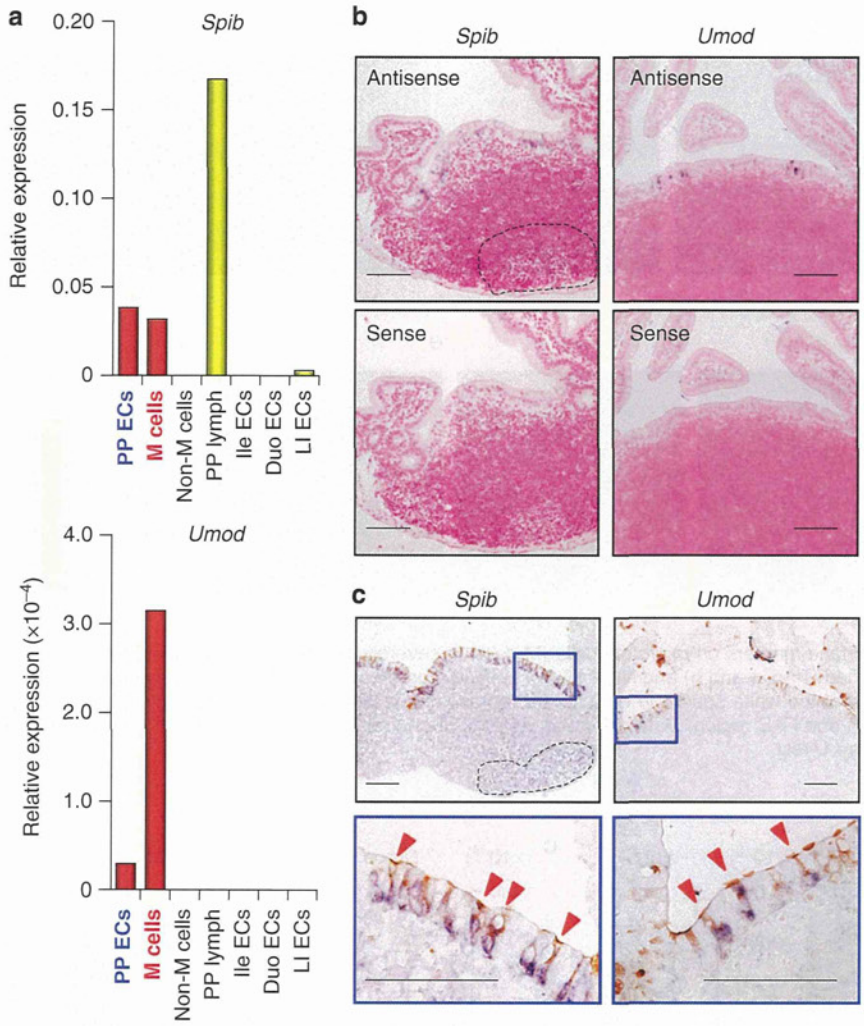

Figure 1 M cells are unique among intestinal epithelial cells in showing expression of *Spib* and *Umod*. (**a**) Real-time PCR analysis of the expression of newly identified M-cell–specific genes in the cell fractions indicated. Each result was normalized against the expression of glyceraldehyde 3-phosphate dehydrogenase (*Gapdh*) and is representative of three independent experiments. Lymph, lymphocytes; Ile, ileal; Duo, duodenal; LI, large intestinal. (**b**) *In situ* hybridization assay to detect *Spib* and *Umod* mRNA in a duodenal PP. Each antisense, but not sense, cRNA probes reacted with FAE regions to give a blue stain. Bar = 100 μm. (**c**) *Spib* and *Umod* signals were merged with brown UEA-1 staining in the FAE region. Each bottom panel is a higher magnification of the blue square in each top panel. Dotted circles found in **b** and **c** indicated germinal center region of PPs. Data are representative of two independent experiments. Bar = 100 μm.

simply been impairment of fucosylation on some M-cell–specific surface molecules. To test this possibility, we assessed the expression of *Fut1* mRNA in the FAE region. Unexpectedly, the levels of *Fut1* expression were comparable in $Spib^{+/+}$ and $Spib^{-/-}$ mice (**Figure 3b**). We further examined the expression of other M-cell–specific genes, including *Umod*, in $Spib^{+/+}$ and $Spib^{-/-}$ mice. Although *Umod*, like *Gp2*, was poorly expressed in $Spib^{-/-}$ FAE, the expression levels of *Marcksl1* (which encodes MARCKS-like protein) and *Pglyrp1* (which encodes peptidoglycan recognition protein S) in the FAE region of $Spib^{-/-}$ mice were similar to those in wild-type mice (**Figure 3c**). These results indicated that M-cell–specific expression molecules could be divided into two groups according to their dependence on Spi-B for gene regulation.

Abundance of cells with irregular and short microvilli is diminished in $Spib^{-/-}$ PPs

M cells are easily distinguished from the neighboring columnar ECs by their morphologically unique surface microvilli, which are sparser and shorter. It is likely that these irregular microvilli are convenient for the effective uptake of ingested antigens from luminal sites in the digestive tract. Therefore, this feature is another hallmark of M cells. We prepared PPs from $Spib^{+/+}$ and $Spib^{-/-}$ mice and then observed and counted hollow cells by scanning electron microscopy. M cells were preferentially found at the edge of the FAE region in wild-type mice as "sunken" cells (**Figure 4a,b**; about 35 sunken cells per 0.01-mm^2 field). In contrast, these sunken cells were rarely detected (about 3 sunken cells per 0.01-mm^2 field) in the corresponding region of $Spib^{-/-}$ mice. Notably, however, a pocket structure

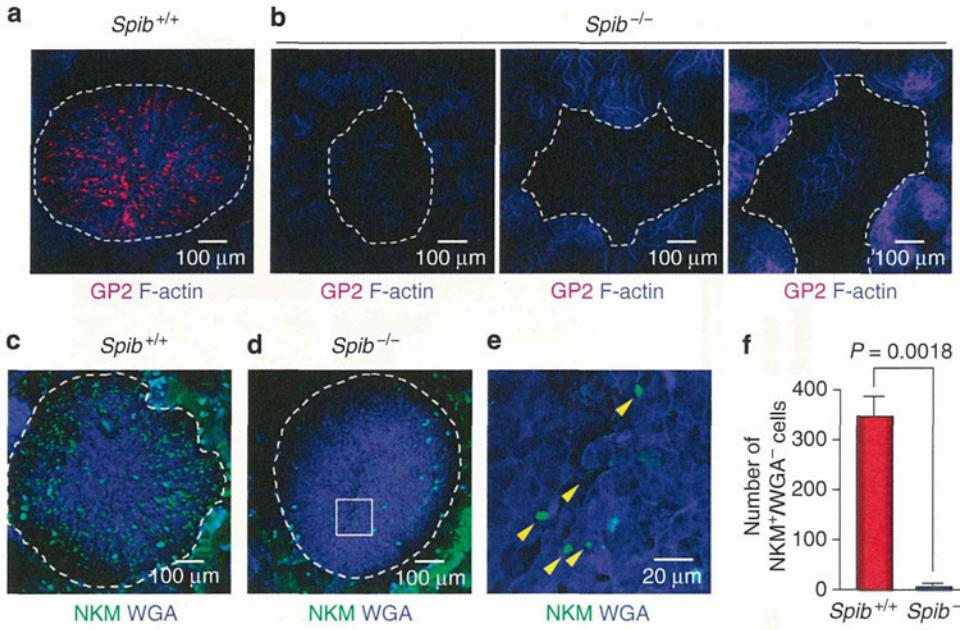

Figure 2 Abundance of surface markers on microfold cells (M cells) is severely diminished in Spi-B–deficient mice. Whole-mount staining analysis using anti-GP2 antibody (red; **a** and **b**) and NKM 16-2-4 antibody (green; **c**–**e**) in PPs from wild-type (**a** and **c**) and *Spib*$^{-/-}$ (**b** and **d**) mice. (**e**) High-magnification image of the white square in **d**. Data are representative of at least three independent experiments. (**f**) The number of NKM^{+} WGA^{-} cells found in one FAE region. Data are mean ± s.e.m. of one representative from three independent experiments. *P*-values were determined by Mann–Whitney *U*-test.

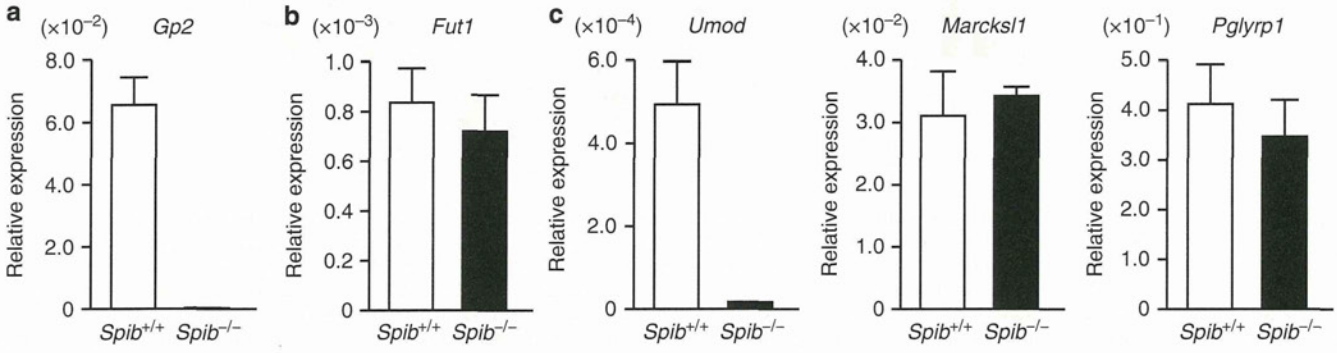

Figure 3 Spi-B–dependent and –independent expression of M-cell–specific genes. Real-time PCR analysis of the expression of several M-cell–specific genes (**a**, *Gp2*; **b**, *Fut1*; and **c**, *Umod*, *Marcksl1*, and *Pglyrp1*) in FAE prepared from *Spib*$^{+/+}$ and *Spib*$^{-/-}$ mice. Each result was normalized against the expression of *Gapdh* and is shown as the mean ± s.d. of one representative from three independent experiments. *P*-values were determined by Student's *t*-test.

enfolding lymphocytes was found in the *Spib*$^{-/-}$ M cells (**Supplementary Figure S2** online), as in the wild-type M cells.[13] These data are consistent with the whole-mount staining data we obtained with NKM/WGA, but not with anti-GP2 antibody (**Figure 2f,b**); they suggest that although the unique surface morphology of most M cells is also regulated by Spi-B, there is a small population of M cells (about 10 per FAE region; **Figure 2f**) of which differentiation is independent of Spi-B.

B-cell–intrinsic Spi-B is dispensable in the induction of M-cell–specific markers

Spib$^{-/-}$ mice showed a severe reduction in M-cell features, but Spi-B is expressed mainly in hematopoietic cells—particularly in B cells and plasmacytoid dendritic cells.[14–16] Moreover, one report has indicated that a certain B-cell subset residing in the subepithelial dome of the PP mucosa contributes to M-cell differentiation.[17] Therefore, we next investigated whether B cells (or T cells, or both) were responsible for the expression of GP2 on M cells. We used bone marrow (BM) chimeric mice, created by transplanting wild-type or *Spib*$^{-/-}$ BM cells into recombination activating protein 1 (RAG1)-deficient mice, which have no mature B and T lymphocytes.[18] The number of GP2^{+} cells in RAG1-deficient mice that received *Spib*$^{-/-}$ BM cells was comparable to the number in those that received wild-type BM cells (**Figure 5**), indicating that Spi-B expressed in B and T cells was not important in inducing or maintaining M-cell surface markers.

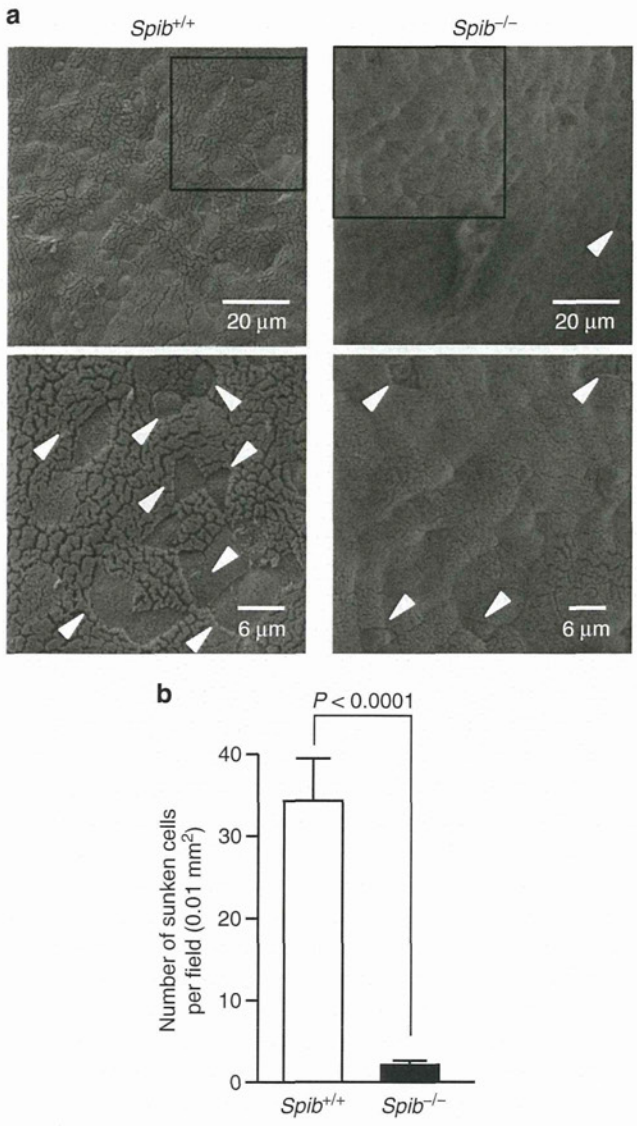

Figure 4 Number of sunken cells in FAE regions is decreased in Spi-B–deficient mice. (**a**) Scanning electron microscopic analysis of duodenal Payer's patch PPs from *Spib*$^{+/+}$ and *Spib*$^{-/-}$ mice. Typical M cells are indicated by arrowheads. Each bottom panel is a higher magnification of the box in each top panel. Data are representative of two independent experiments. (**b**) Calculated numbers of sunken cells per field. Data are means ± s.e.m. of one experiment representative of two independent experiments. *P*-values were determined by the Mann–Whitney *U*-test.

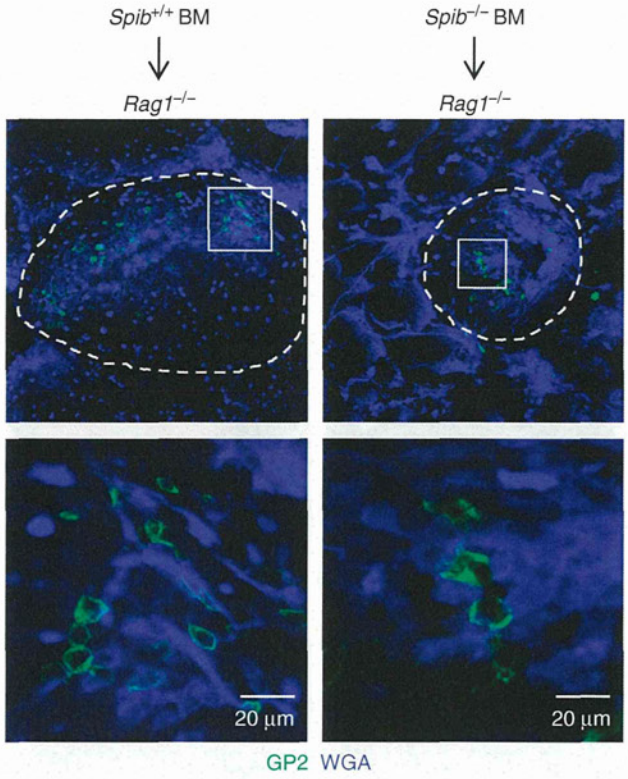

Figure 5 Spi-B expressed in B and T cells is not important for the expression of GP2 on M cells. Bone marrow (BM) cells were prepared from *Spib*$^{+/+}$ and *Spib*$^{-/-}$ mice and then transferred to RAG1-deficient mice. At 8 weeks after the transfer, GP2-positive FAE cells were visualized by whole-mount staining using anti-GP2 antibody (green). WGA was used for epithelial-cell counterstaining (blue). Each bottom panel is a higher magnification of the white square in each top panel. Data are representative of two independent experiments.

M cells differentiated by an Spi-B–independent pathway can transcytose PP-resident bacteria

M cells are specialized for antigen uptake.[1] Although small numbers of M cells were observed in the FAE region in *Spib*$^{-/-}$ mice (fewer than 5% of those in the wild type), it seemed that most M-cell features, such as expression of surface markers and apical morphology, were diminished in these mice. These findings raise the possibility that *Spib*$^{-/-}$ mice have diminished uptake of pathogenic or opportunistic bacteria, or both. Consistent with the loss of GP2 expression, uptake of *Salmonella* Typhimurium, which depends on host GP2 for binding to M cells, was markedly lower in *Spib*$^{-/-}$ mice than in wild-type mice (**Supplementary Figure S3** online).

We further examined whether PPs of *Spib*$^{-/-}$ mice possessed *Alcaligenes* spp., which, as we recently discovered, are opportunistic bacteria that inhabit inside PPs;[19] *Alcaligenes* spp. were moved from the lumen of the small intestine to the inside of the PPs preferentially via PP M cells (**Figure 6a**). Consistent with our previous reports,[19,20] *Alcaligenes* spp. had colonized the inside of the PPs well in wild-type mice (**Figure 6b**). Interestingly, intratissue *Alcaligenes* spp. were also detected inside the PPs from *Spib*$^{-/-}$ mice at levels almost comparable to those found in wild-type PPs (**Figure 6b**). Next, we examined *Alcaligenes* uptake capability in the PPs of *Spib*$^{-/-}$ mice by ligated-intestinal loop assay using culturable *A. faecalis*. Although *Spib*$^{-/-}$ mice showed a tendency toward reduced uptake, there was no significant difference between *Spib*$^{+/+}$ and *Spib*$^{-/-}$ mice in the translocation of *Alcaligenes* to the inside of the PPs (**Figure 6c**). These data indicated that *Alcaligenes* spp. could move to, and inhabit, the inside of the PPs, even if the host lacked Spi-B–dependent M cells.

DISCUSSION

In this study, we identified the novel M-cell–specific expression genes *Umod* and *Spib*. Spi-B-deficient mice showed complete